Exposure Fluctuations of Astronauts Due to Orientation

John W. Wilson, John E. Nealy,
James S. Wood, Gary Qualls,
William Atwell, Judy L. Shinn,
and Lisa C. Simonsen

NASA

Exposure Fluctuations of Astronauts Due to Orientation

John W. Wilson and John E. Nealy
Langley Research Center
Hampton, Virginia

James S. Wood and Gary Qualls
FMC, Inc.
Hampton, Virginia

William Atwell
Rockwell Aerospace
Houston, Texas

Judy L. Shinn and Lisa C. Simonsen
Langley Research Center
Hampton, Virginia

Abstract

The dose incurred in an anisotropic environment depends on the orientation of the astronaut's body relative to the direction of the radiation field. The fluctuations in exposure of specific organs due to astronaut orientation are found to be a factor of 2 or more in a typical space habitation module and typical space radiations. An approximation function is found that overestimates astronaut exposure in most cases studied and is recommended as a shield design guide for future space missions.

Introduction

There are many uncertainties that enter into estimates of biological risk to astronauts in deep space that must be managed to ensure astronaut radiation exposure risk in future missions does not exceed acceptable limits. These uncertainties are from several sources: (1) the external environment, (2) modification of the external environment by shielding materials, (3) the shielding geometry models, (4) computational methods for estimating the internal environment of the spacecraft, (5) interaction of the interior environment with the human body, (6) the body geometry, (7) computational procedures for relating the internal environment to exposure of specific tissues, and (8) the biological response to specific tissue exposures.

Environmental uncertainties arise from the galactic cosmic ray (GCR) models used and the unpredictable nature of solar particle events (SPE). Improvements in GCR models are in progress (ref. 1), but SPE exposures will remain unpredictable into the foreseeable future (ref. 2). A maximum observed SPE fluence event is usually used for design purposes (ref. 3). This is not to say that these fluence levels may not be someday exceeded but rather that no observed event has exceeded them in the past.

The uncertainty in the shielding properties of materials is not accurately known for HZE components. Significant uncertainty is known to result from the choice of nuclear models (ref. 4). Uncertainty in shielding properties for the biologically most significant components on the order of 200 percent has been estimated on the basis of physical limits on reaction mechanisms (ref. 5). A further computational uncertainty caused by assuming that nuclear cross sections for HZE fragmentation are energy independent adds an additional 50 percent uncertainty (ref. 6).

The geometry of the spacecraft structure is never exactly represented and even varies throughout the mission as expendables are consumed. Three-dimensional aspects of the solution to the Boltzmann equation have been simplified and boundary conditions have never been exactly matched (refs. 7 and 8). However, conservative methods are normally employed that rarely cause significant errors (ref. 8). The interior environment is rarely evaluated at more than a few specific locations so that the boundary flux (including leakage) at the surface of the astronaut's body is never exactly specified (refs. 8 and 9). There is further uncertainty in the interaction with the body tissues (ref. 10) and specification of the body geometry (ref. 11). Finally, the biological response to many of the environmental components is largely unknown (refs. 3, 12, and 13). Clearly, all of these factors must be dealt with in a consistent fashion to ensure astronaut safety in future deep-space missions. In the present report, we endeavor to consider uncertainty associated with astronaut geometric factors (specifically, astronaut orientation).

If the radiation fields to which the astronaut is exposed are isotropic, then the exposure of specific organs is independent of the astronaut orientation. Radiations within the geomagnetic field are anisotropic, since particle motion is strongly affected by the local magnetic field direction. Even outside the geomagnetic field where galactic and solar cosmic rays are nearly isotropic, the astronaut is enclosed within a large spacecraft of a complicated geometric shape in which the interior radiation fields are highly anisotropic. The radiation anisotropy is related to the distribution of material about the radiation field point.

As a practical example, we consider a representative habitation module as illustrated in figure 1. The module configuration is defined by a computer-aided design (CAD) model based on early Space Station *Freedom* layouts and includes racks, end plates, windows, utility raceways, and the pressure vessel walls. Appropriate nominal densities have been assigned to each of the constituents. Three interior points along

the centerline have been chosen for dose analysis: (1) in the end (windowed) section least protected by inherent shielding, (2) near the geometric center where maximum shielding exists, and (3) at the opposite end location where intermediate shielding exists. These points will be referred to as A, B, and C, respectively. Directional thickness data prescribed in a three-dimensional reference frame must be used to examine the effects of differing orientations at a given location in the spacecraft. Figure 2 shows such directional thickness patterns for the specified target points in the CAD-modeled habitation module. It is apparent that the central location offers greatest protection, while positions near the end walls are associated with smaller thickness values in directions facing away from the center region. Shadowing due to utility raceways, racks, and end plates is also prominent in the illustrations. The directional patterns are based on thicknesses along 1922 rays evenly distributed about the target point with respect to solid angle.

The NASA computerized anatomical man (CAM) model (ref. 11) is used to define the astronaut geometry. Directional thickness patterns for the selected human body target points are shown in figure 3. The pattern for the skin at a central chest location exemplifies the contrast between the most shielded directions and the most exposed directions, which results in two approximate hemispherical patterns (blue in front and pink in back). The distribution about the right-eye location also indicates a large solid angle of high exposure, but noticeable asymmetry exists because of the off-axis position of this target. The thyroid and esophagus distributions are indicative of intermediate self-shielding locations, and the intestine point represents that for which most self-shielding is available. The CAM model distributions are derived from a 512-ray pattern, and while the directional resolution is not as good as for the habitat module, the thickness patterns are generally defined well enough to make important features readily identifiable. The patterns in figure 3 are oriented so that the head location is toward the top of the direction sphere; the frontal direction is indicated by the position of the solid angle for which least thickness occurs.

It is clear that the exposure at a location in the astronaut's body depends on the distribution of the vehicle structure mass and the astronaut's body mass about the exposure point. How the two mass distributions combine depends on the relative orientation of the astronaut. The importance of this orientation on evaluating astronaut exposure is the object of the current study.

Dose Within Convex Regions

It can be shown (ref. 8) that the dose from proton or ion exposure within a convex region can be approximated (conservatively) by

$$D(\vec{x}) = \iint R[E, t_x(\vec{\Omega})]\, \Phi(E, \vec{\Omega})\, d\vec{\Omega}\, dE \qquad (1)$$

where $R(E, Z)$ is the solution for the normally incident beam of particles of energy E in slab geometry at a depth Z, and $\Phi(E, \vec{\Omega})$ is the fluence density of ions of energy E moving in direction $\vec{\Omega}$. The distribution of shield material about the dose point $\vec{x}$ is defined by the areal density distribution $t_x(\vec{\Omega})$.

In the case of a monodirectional beam, the dose according to equation (1) is

$$D_{\vec{\Omega}_B}(\vec{x}) = \int \Phi(E) R[E, t_x(\vec{\Omega}_B)]\, dE \qquad (2)$$

where $\vec{\Omega}_B$ is the radiation direction. If we randomly reorient the body relative to the direction of irradiation, the dose fluctuates at $\vec{x}$ according to the distribution of areal density about $\vec{x}$ given by $f_x(t)\, dt$. Note that $f_x(t)\, dt$ is the probability for an arbitrarily chosen direction that the shield thickness lies between t and $t + dt$. The NASA CAM model (ref. 11) has been used to provide thickness cumulative distribution functions (cdf's) and probability density functions (pdf's) for selected human body exposure locations. The body target points for this study have been chosen to represent varying degrees of body self-shielding. In order of increasing amount of self-shielding, the five selected locations are (1) skin in chest region, (2) right ocular lens, (3) thyroid gland, (4) esophagus, and (5) central intestinal point. The respective thickness distributions are shown in

figures 4(a)–(e). The peak value of the pdf at each body target point is an indicator of relative effective self-shielding. The mean dose for all orientations is evaluated by using a code developed by Shinn et al. (ref. 6) as

$$\overline{D}_x = \iint \Phi(E) R[E, t_x(\vec{\Omega}_B)] \, d\vec{\Omega}_B \, dE = \iint \Phi(E) R(E, t) f_x(t) \, dt \, dE \tag{3}$$

the standard deviation of dose, σ_o, is given by

$$\sigma_o^2 = \iint [\Phi(E) \, R(E, t)]^2 f_x(t) \, dt - \overline{D}_x^2 \tag{4}$$

A crude approximation of the dose fluctuations can be taken as

$$f_{D_x}(D) = \frac{1}{\sqrt{2\pi}\sigma_o} \exp\left[-\frac{(D - \overline{D}_x)^2}{\sigma_o^2} \right] \tag{5}$$

Also important in interpreting this approximate distribution is the maximum dose and minimum dose associated with directions $\vec{\Omega}_{B_{\max}}$ and $\vec{\Omega}_{B_{\min}}$ in equation (2). The cumulative distribution is taken as

$$F_{D_x}(D) = \frac{\int_{D_{\min}}^{D} f_{D_x}(D') \, dD'}{\int_{D_{\min}}^{D_{\max}} f_{D_x}(D') \, dD'} = \frac{\mathrm{erf}[(D - \overline{D})/(\sqrt{2}\sigma_o)] - \mathrm{erf}[(D_{\min} - \overline{D})/(\sqrt{2}\sigma_o)]}{\mathrm{erf}[(D_{\max} - \overline{D})/(\sqrt{2}\sigma_o)] - \mathrm{erf}[(D_{\min} - \overline{D})/(\sqrt{2}\sigma_o)]} \tag{6}$$

The distribution given by equation (6) is to be compared with the distribution at several typical locations within critical organs of the human body. The integral

$$D_{\mathrm{slab}}(t) = \int_0^\infty \Phi(E) \, R(E, t) \, dE \tag{7}$$

is replaced by a trial function as

$$D_{\mathrm{slab}}(t) = D_o \exp(-\alpha t) \tag{8}$$

where the e-folding distance is α^{-1} and $0.04 \leq \alpha \leq 0.4$ brackets the observed solar spectra. We arbitrarily set D_o to 100 cSv.

The cumulative distribution of exposure for the most penetrating exposure ($\alpha = 0.04$ cm^2/g) is shown in figure 5. Equation (6) is seen to be a poor approximation for the least shielded dose points but improves for dose points in tissues deeper in the astronaut's body. Results for the least penetrating radiations ($\alpha = 0.4$ cm^2/g) shown in figure 6 exhibit large deviations from equation (6) at all tissue locations. Similar results are shown for a very lightly shielded astronaut during the solar particle events of October 1989 and February 1956 in figures 7 and 8. In general, the exposure fluctuations in this case of monodirectional environments are not well represented by normal statistics, and the standard deviation has no clear meaning, even in the restricted sense of equation (6).

Astronaut Exposure Within a Spacecraft

In the case of isotropic radiation exposure, one may rewrite equation (1) as

$$D(\vec{x}) = \int \Phi(E) \, dE \int R[E, t_x(\vec{\Omega})] \, d\vec{\Omega} \tag{9}$$

for which the fractional solid angle distribution may be introduced as

$$D(\vec{x}) = 4\pi \int \Phi(E) \, dE \int_0^\infty R(E, t) \, f_x(t) \, dt \tag{10}$$

3

where $f_x(t)\,dt$ is the solid angle fraction with $t(\vec{\Omega})$ lying between t and $t + dt$. Note $f_x(t)$ is related to the directional thickness distribution of the previous section. The dose in the center of a sphere is found by taking $f_x(t)$ to be $\delta(t - r)$ so that

$$D_{sp}(r) = 4\pi \int \Phi(E)\,dE\,R(E, r) \tag{11}$$

from which the dose at a point $\vec{x}$ in arbitrary geometry can be written as

$$D(\vec{x}) = \int D_{sp}(t)\,f_x(t)\,dt \tag{12}$$

The error generated by equation (9) is second order in the ratio of beam divergence to radius of curvature of the exposed object and is always conservative (refs. 7 and 8). Note that equation (11) approximates the dose in the center of a sphere by the dose in a slab for which all the radiation is incident normally on the exterior surface. Obviously, such an assumption is conservative since leakage at the sphere boundary is underestimated in slab geometry but approaches the slab as the sphere radius becomes large (ref. 8).

If the convex body is allowed to rotate to a new position defined by a colatitude and azimuth, then the integral of equation (1) becomes

$$D(\vec{x}) = \iint R\{E, t_x[R_y(\theta)\,R_z(\phi)\,\vec{\Omega}]\}\,\Phi(E, \vec{\Omega})\,d\vec{\Omega} \tag{13}$$

where $R_y(\theta)$ and $R_z(\phi)$ are rotation operators (ref. 14).

The average exposure for all orientations is then

$$\overline{D}(\vec{x}) = \frac{1}{4\pi} \iiint R\{E, t_x[R_y(\theta)\,R_z(\phi)\,\vec{\Omega}]\}\,\Phi(E, \vec{\Omega})\,d\vec{\Omega}\,d\vec{\Omega}' = \iint R(E, t)\,\Phi(E, \vec{\Omega})\,d\vec{\Omega}\,f_x(t)\,dt \tag{14}$$

which shows that a randomly rotating body exposure is equivalent to assuming the omnidirectional flux is isotropic.

Suppose a region b is to be protected by enclosing it within a region s; then the dose at a point $\vec{x}$ within b is

$$D(\vec{x}) = \iint R[E, t_s(\vec{\Omega}) + t_b(\vec{\Omega})]\,\Phi(E, \vec{\Omega})\,dE\,d\vec{\Omega} \tag{15}$$

where we assume the body and shield are constructed of the *same* material. Otherwise, $R(E, t)$ must be replaced by the more complicated functions derived as buildup factors in reference 7. If the body is randomly rotated within the shield, then

$$D(\vec{x}) = \iint R[E, t_s(\vec{\Omega}) + t_b]\,f_b(t_b)\,dt_b\,\Phi(E, \vec{\Omega})\,dE\,d\vec{\Omega} \tag{16}$$

which may be reduced for isotropic exposure to

$$D(\vec{x}) = 4\pi \iint R(E, t_s + t_b)\,f_s(t_s)\,f_b(t_b)\,\Phi(E)\,dE\,dt_b\,dt_s = \int D_{sp}(t) \int f_s(\tau)\,f_b(t - \tau)\,dt\,d\tau \tag{17}$$

Note that from equation (17), we define a combined areal density distribution function as

$$f_{sb}(t) = \int f_s(\tau)\,f_b(t - \tau)\,d\tau \tag{18}$$

which is valid for a randomly rotating inner body shielded by a distribution $f_s(t_s)$ in an isotropic environment.

4

Optimum Shield Design

The environment in deep space can be assumed to be isotropic in most cases. One may represent the dose in a convex body as an integral of the dose in variable-radius spheres as

$$D(\vec{x}) = \int D_{sp}(r)\, f_b(r)\, dr \qquad (19)$$

where we overestimate the sphere dose by dose in a slab. We consider a series of shapes with the same average thickness

$$\bar{t} = \int t\, f_b(t)\, dt \qquad (20)$$

so we may ask which shape gives minimum exposure to the dose point. We model this question by assuming a class of distributions for the cardioid given as

$$F_b(t) = \left\{ \begin{array}{ll} (t - \bar{t} + \delta)/2\delta & (\bar{t} - \delta \le t \le \bar{t} + \delta) \\ 0 & \text{(Otherwise)} \end{array} \right\} \qquad (21)$$

where $F_b(t)$ denotes the cumulative distribution function. We may then ask which of the doses for the areal density distribution given by equation (21) as a function of δ is least. The dose in the center of a sphere decreases (approximately) as an exponential for most space radiations (see eq. (8)) for which

$$D(\vec{x}) = D_{sp}(\bar{t}) \left(1 + \frac{1}{3!}\alpha^2\delta^2 + \frac{1}{5!}\alpha^4\delta^4 + \cdots \right) \qquad (22)$$

where α^{-1} is the e-folding distance of $D_{sp}(t)$. The dose increases monotonically with increasing δ and is minimum at $\delta = 0$, where the variation in δ is likewise zero. The optimum shield configuration is a sphere (spherical shell) whose radius is the mean thickness. Note that $D(\vec{x})$ changes rapidly with δ for $\delta \gg \alpha^{-1}$ but is relatively insensitive to changes in shape for $\delta \ll \alpha^{-1}$. Highly penetrating radiations (α small) are less sensitive to nonspherical shapes, while low penetration events (α large) require δ to be small for optimum shielding.

It has been tempting in the past to assume that the dose at $\vec{x}$ can be estimated by the dose in the center of a sphere of the same average thickness. Clearly, this is an underestimate for most practical problems and should be *avoided*, since astronaut exposure would always exceed design values. We may also conclude that the exposure is maximum in the center of a spherical-shell shield and decreases as one approaches the walls, since the minimum thickness is fixed and the average thickness increases as the wall is approached.

Although the areal density distribution functions contain no specific information on orientation, we may nonetheless use them to provide an upper and lower bound on exposure. The dose within a body in a shielded region is given by equation (15). If the body is reoriented by rotations (θ, ϕ) then

$$D(\vec{x}) = \iiint R\{E, t_s(\vec{\Omega}) + t_b[R_y(\theta)\, R_z(\phi)\, \vec{\Omega}]\}$$
$$\times\ \Phi(E, \vec{\Omega})\, dE\, d\vec{\Omega} \qquad (23)$$

Clearly, $D(\vec{x})$ depends on the orientation angles. For an isotropic environment as is usually found in deep space,

$$D(\vec{x}) = \int D_{sp}\{t_s(\vec{\Omega}) + t_b[R_y(\theta)\, R_z(\phi)\, \vec{\Omega}]\}\, d\vec{\Omega} \quad (24)$$

For a given set of angles (θ, ϕ) there is a unique areal density distribution for which

$$D(\vec{x}) = \int D_{sp}(t)\, f_{sb}(t, \theta, \phi)\, dt \qquad (25)$$

Clearly, the minimum exposure occurs when θ and ϕ are chosen to best approach spherical symmetry and maximum exposure when the maximum deviation from spherical symmetry occurs. It is obvious that the average thickness $\langle t_s + t_b \rangle$ is independent of orientation, but the thickness standard deviation σ could change considerably. If σ approaches zero, then $D(\vec{x}) \approx D_{sp}(\bar{t})$; a large σ yields

$$D(\vec{x}) = D_{sp}(\bar{t}) \left(1 + \frac{1}{2}\alpha^2(\sigma)^2 + \cdots \right) \qquad (26)$$

showing the minimum variance to be the optimum configuration and the maximum variance to be the worst-case exposure.

Strictly speaking, the areal density distributions contain no specific directional information. However, we may seek combinations of areal densities for which the variance is either minimized or maximized corresponding to bounds on the body exposure due to orientation. As was shown earlier, the average over all orientations is given by the convolution as

$$\bar{f}_{sb}(t) = \frac{1}{4\pi} \int f_{sb}(t, \theta, \phi)\, d\vec{\Omega}$$

$$= \int_0^t f_s(\tau)\, f_b(t - \tau)\, d\tau \qquad (27)$$

The maximum variance combination F_u is found by matching the solid angles with least thickness and the solid angles with maximum thickness for each of the two regions. Obviously, this assumes high angular correlation of the two thickness distributions. Thus, F_u is the combined solid angle fraction with thickness less than $t = t_b + t_s$, where t_b and t_s are given as solutions of

$$F_b(t_b) = F_u(t) \qquad (28)$$

$$F_s(t_s) = F_u(t) \qquad (29)$$

and $F_b(t_b)$ and $F_s(t_s)$ are the cumulative distributions for the body and shield. Similarly, assuming good angular correlation, the minimum variance combination $F_L(t)$ is found from

$$F_b(t_b) = 1 - F_L(t) \qquad (30)$$

$$F_s(t_s) = F_L(t) \qquad (31)$$

where $t = t_s + t_b$ as before. Note that the upper and lower limits given by equations (28) to (31) would correspond most closely to the 3σ limits of a normal distribution. The mean exposure is given by the convolution in equation (27).

It is clear in the above constructions that the mean thickness is preserved in each case. The standard deviation of the combined thickness distribution is, however, quite distinct. It can be shown that the standard deviation of thickness for a randomly rotated, inner body is

$$\sigma_{sb} = \left(\sigma_s^2 + \sigma_b^2\right)^{1/2} \qquad (32)$$

corresponding to the distribution of equation (27). The standard deviation of the combined mass distribution for maximum exposure given by equations (28) and (29) is

$$\sigma_{sb} = \sigma_s + \sigma_b \qquad (33)$$

The minimum exposure standard deviation is given as

$$\sigma_{sb} = |\sigma_s - \sigma_b| \qquad (34)$$

corresponding to equations (30) and (31). If we assume the dose attenuation function of equation (8) and further assume the thickness distributions $f_s(t)$ and $f_b(t)$ are normal, then the mean dose for all orientations is

$$\overline{D} = D_o \exp\left\{-\alpha\left[\bar{t} - \left(\sigma_s^2 + \sigma_b^2\right)\frac{\alpha}{2}\right]\right\} \qquad (35)$$

According to equations (33) and (34), the dose standard deviation with orientation is

$$\sigma_o \approx \frac{\overline{D}}{3}\sigma_s\sigma_b\alpha^2\left(1 + \frac{\sigma_s^2\sigma_b^2\alpha^4}{6} + \cdots\right) \qquad (36)$$

Although the distributions are generally far from normal, the procedure above provides insight into the major factors in dose fluctuations.

Astronaut in a Habitat

We now apply the procedures to the case of an astronaut in a space habitation module. The habitation module used is an early Space Station *Freedom* design shown in figure 1. For simplicity, we consider only the three locations in the module denoted by A, B, and C as discussed previously. The thickness distributions about the points are shown in figures 2 and 9. For each of the three target points, thickness cumulative distribution functions (cdf's) have been determined from which corresponding probability density functions (pdf's) are obtained by differentiation. These distribution functions for the selected interior points in figure 1 are shown in figures 9(a)–(c). Peak values of the pdf's and median (50 percentile) values of the cdf's are indicative of effective shielding at each location. It is readily seen that the most protection exists for point B, while the largest exposures are to be expected at point A.

Thickness distributions for the human body within the habitat module may then be constructed for combinations of the cdf's in figures 4 and 9 to provide maximum and minimum variance distributions as has been described by equations (28)–(31). In addition, the distribution corresponding to random orientation may be obtained from the convolution of the module and body pdf's (eq. (27)). The set of combined pdf's may then be used in conjunction with appropriate dose-versus-depth functions to compute the doses to the selected organs at each of the points in the spacecraft structure. Thus, for each combination of body point and position in the module, values for a mean (convolution) dose and a range (minimum, maximum) are found.

Dose-versus-depth functions corresponding to three values of e-folding coefficients that represent flux spectra of high, moderate, and low penetrability ($\alpha = 0.04$, 0.1265, and 0.4, respectively) have been used in the analysis (eq. (8) with $D_o = 100$ cSv). In addition, dose-versus-depth functions corresponding to the observed proton spectra for the solar particle events that occurred in February 1956 (very penetrating) and in the autumn of 1989 (moderately penetrating) have been included in the analysis. The

dose-versus-depth functions as computed with the Langley BRYNTRN (ref. 15) code for the observed spectra are shown in figure 10.

While the dose quantities evaluated from the thickness distribution functions can provide a mean and an absolute range, no direct information regarding variability associated with directional orientation is available. Directional distribution of the internal radiation field can be derived from the thickness distributions at the three designated locations in the habitation module shown in figure 2.

Directional dose patterns projected on the unit sphere are shown in figures 11 and 12. Note that the color scale for relative dose values is the inverse of that for the distributions of thickness. Figure 11 illustrates the dose pattern in the habitation module at target point A for the attenuation coefficients for high, moderate, and low penetrability dose-versus-depth functions. Shadowing from end-plate structure and utility raceways is evident. Also prominent in this view are the three window locations, which are areas of higher mass density than the surrounding wall structure.

Figure 12 illustrates dose patterns for CAM model body points as computed from the 1989 proton flare dose-versus-depth function. Shown are the directional distributions about the right eye, thyroid, and intestinal track locations, representing points receiving very high, moderate, and relatively low exposures, respectively.

The three-dimensional-thickness distributions (illustrated in figs. 2 and 3) allow one to compute dose to a specified body target point at a given location in the module for any arbitrary alignment of relative orientation. Thus, a distribution of dose values may be obtained that provides not only a mean and an absolute range, but also a variance and "practical" range of exposure values. Such information has been obtained in the present study by constructing an algorithm that utilizes a uniform random number distribution to generate statistics on dose values obtained at various orientations of the body organ points relative to the vehicle orientation (see appendix). It was determined (principally by trial and error) that 512 random orientations would provide adequate statistics to define a given distribution of dose values. This procedure was performed for the combinations of selected body points at the three locations in the habitat configuration for the five representative dose-versus-depth functions. These results are summarized in figures 13(a)–(e), 14(a)–(e), and 15(a)–(e), which relate to calculations at points A, B, and C in the habitat, respectively.

Results for each case are presented as dose values grouped in 25 bins, along with a spline-fit function through the binned data. The ordinate for each plot is scaled so that the integrated value is unity and thus represents a probability density in dose for random orientation. A bar inserted along each abscissa is divided into six segments that indicate 1σ, 2σ, and 3σ values on either side of the calculated mean. Scrutiny of the absolute range values (D_{min}, D_{max}) for each case, as computed from the cumulative thickness distributions, has indicated that an approximate "practical" dose range, ΔD_p, may be obtained as

$$\frac{\overline{D} - D_{min}}{2} < \Delta D_p < \frac{\overline{D} + D_{max}}{2} \qquad (37)$$

where $\overline{D}$ is the mean determined from the convolution integral of the body organ and habitat pdf's. These "practical" dose ranges are indicated on the plots as open symbols above the 3σ range bars. The open diamond represents the convoluted value for mean dose, and the limits of practical range are indicated by the inverted triangles. In most cases, the "practical" range gives a reasonable approximation to the range of the actual dose distribution, which may be especially large for some flare spectra. For example, results for exposures at point A due to the fall 1989 spectrum (fig. 13(d)) indicate dose fluctuations by factors of 2 or more about the mean value for several body target points. As may be seen in the results for point B (fig. 14), this approximation tends to become conservative when the distribution is sharp (i.e., peaked about a narrow range). The upper limit of the practical range provides a conservative dose estimate for shield design and is rarely exceeded in application.

Observed differences in the analytic convolution and mean values calculated from the random orientation statistics are attributable both to numerical error in performing the convolution integrations and to the finite number of random orientations included in each case. Clearly, these differences are minor and are indicative of the adequacy of the orientation statistics. In all cases, the variation of dose with body self-shielding is consistent for the progression between the skin location and the internal intestinal point. The impact of spectral hardness at each habitat location may be seen in parts (a), (b), and (c) of figures 13–15. Parts (d) and (e) give results for observed flare spectra. In particular, one may note the large impact that location in the habitat has on skin and eye doses for the 1989 flare spectrum, which may be compared with the markedly reduced sensitivity for the much harder February 1956 spectrum.

Concluding Remarks

The variability of exposure (incurred radiation dose equivalent D) during a large solar particle event for an astronaut in a space habitation module is examined. A formal analytical development is presented that treats the dose fluctuations in terms of relevant thickness distributions and radiation spectral parameters. The general formalism is then applied to computerized geometric models of the human body in combination with a simulated space habitation module configuration. Calculations of average dose values and associated upper and lower bounds are illustrated for idealized dose-versus-depth functions, as well as for functions derived from observed large proton flare spectra. Computational cases considered include interior spacecraft locations that were heavily, moderately, and lightly shielded, with thickness distributions representative of conceptual future space habitation modules. Five locations within a geometric model of the human body were also considered in the analysis and typified varying degrees of body self-shielding.

In order to compare actual dose distribution functions with the theoretical means and bounds, statistical computations were performed for sets of random orientations of the various three-dimensional geometries. It was found that, in general, the actual, or practical, range of variability was substantially less than the absolute range. Examination of the data has indicated that an approximate realistic range may be obtained from the cumulative thickness distributions. Application of this technique could provide reasonable estimates of incurred dose variability with minimal computational effort for a wide variety of space exposure situations. Such analyses should considerably facilitate the further evaluation of estimated risks due to solar particle event exposures. It is recommended that the quantity $(\overline{D} + D_{\mathrm{max}})/2$ be used in shield-design studies to ensure that design exposure limits are not exceeded in actual practice.

Appendix

Rotation Representations of Astronaut Orientation

This appendix gives the details on the relationship between the thickness distributions of dose points in the astronaut to the thickness distribution of the vehicle. The areal density about a point $\bar{x}$ is given as $t_x(\vec{\Omega})$ and is fixed to an astronaut reference frame for which aircraft standards are used (that is, $\hat{z}$ vertically down, $\hat{x}$ forward, and $\hat{y}$ out the right "wing"). The orientation angles will be taken as standard yaw (ψ), pitch (θ), and roll (ϕ). The areal density for the point $\vec{x}$ in the vehicle frame is then

$$t_x[R_x(\phi)\, R_y(\theta)\, R_z(\psi)\, \vec{\Omega}]$$

We represent the rotation operation in terms of direction cosines as

$$\vec{\Omega}_y = R_x(\phi)\, R_y(\theta)\, R_z(\psi)\, \vec{\Omega} \qquad (\text{A1})$$

where R represents the usual rotation matrices (ref. 14). The three angles can be chosen for a fixed astronaut orientation or represented through statistical sampling for which uniform distributions are used as

$$\psi \in U(0, 2\pi)$$

$$\cos\theta \in U(-1, 1)$$

and

$$\phi \in U(0, 2\pi)$$

Future work will examine the statistical fluctuations of organ doses for an astronaut in a habitat such as Space Station *Freedom*.

References

1. Badhwar, G. D.; and O'Neill, P. M.: An Improved Model of Galactic Cosmic Radiation for Space Exploration Missions. Johnson Space Center paper presented at the Second International Cosmic Ray Conference (Dublin, Ireland), Aug. 1991.

2. Smart, D. F.; and Shea, M. A.: Solar Proton Events During the Past Three Solar Cycles *J. Spacecr. & Rockets*, vol. 26, no. 6, Nov.–Dec. 1989, pp. 403 415.

3. Wilson, John W.; Nealy, John E.; and Schimmerling, Walter: *Effects of Radiobiological Uncertainty on Shield Design for a 60-Day Lunar Mission.* NASA TM-4422, 1993.

4. Wilson, John W.; Townsend, Lawrence W.; and Badavi, Forooz F.: Galactic HZE Propagation Through the Earth's Atmosphere. *Radiat. Res.*, vol. 109, no. 2, Feb. 1987, pp. 173–183.

5. Townsend, Lawrence W.; Cucinotta, Francis A.; Shinn, Judy L.; and Wilson, John W.: *Effects of Fragmentation Parameter Variations on Estimates of Galactic Cosmic Ray Exposure Dose Sensitivity Studies for Aluminum Shields.* NASA TM-4386, 1992.

6. Shinn, Judy L.; John, Sarah; Tripathi, Ram K.; Wilson, John W.; Townsend, Lawrence W.; and Norbury, John W.: *Fully Energy-Dependent HZETRN (A Galactic Cosmic-Ray Transport Code).* NASA TP-3243, 1992.

7. Wilson, John W.; Townsend, Lawrence W.; Schimmerling, Walter; Khandelwal, Govind S.; Khan, Ferdous; Nealy, John E.; Cucinotta, Francis A.; Simonsen, Lisa C.; Shinn, Judy L.; and Norbury, John W.: *Transport Methods and Interactions for Space Radiations.* NASA RP-1257, 1991.

8. Wilson, John W.; and Khandelwal, G. S.: Proton Dose Approximation in Arbitrary Convex Geometry. *Nucl. Technol.*, vol. 23, no. 3, Sept. 1974, pp. 298 305.

9. Atwell, W.: Solar Particle Dose Rate Build-Up and Distribution in Critical Body Organs. Paper presented at NATO Advanced Study Institute Conference on Biological Effects and Physics of Solar and Galactic Cosmic Radiation (Armacão de Pêra, Algarve, Portugal), Oct. 12–23, 1991.

10. Schimmerling, Walter: Ground-Based Measurements of Galactic Cosmic Ray Fragmentation in Shielding. Paper presented at the 28th Plenary Meeting of COSPAR (The Hague, The Netherlands), June 25 July 6, 1990.

11. Billings, M. P.; and Yucker, W. R.: *The Computerized Anatomical Man (CAM) Model.* NASA CR-134043, 1973.

12. National Council on Radiation Protection and Measurements: *Guidance on Radiation Received in Space Activities.* NCRP Rep. No. 98, July 31, 1989.

13. Schimmerling, Walter: Radiobiological Problems in Space An Overview. *Radiat. & Environ. Biophys.*, vol. 31, 1992, pp. 197 203.

14. Wilson, John W.: *Analysis and Mechanization of Three- and Four-Gimbal Systems.* NASA TN D-4689, 1968.

15. Wilson, John W.; Townsend, Lawrence W.; Nealy, John E.; Chun, Sang Y.; Hong, B. S.; Buck, Warren W.; Lamkin, S. L.; Ganapol, Barry D.; Khan, Ferdous; and Cucinotta, Francis A.: *BRYNTRN: A Baryon Transport Model.* NASA TP-2887, 1989.
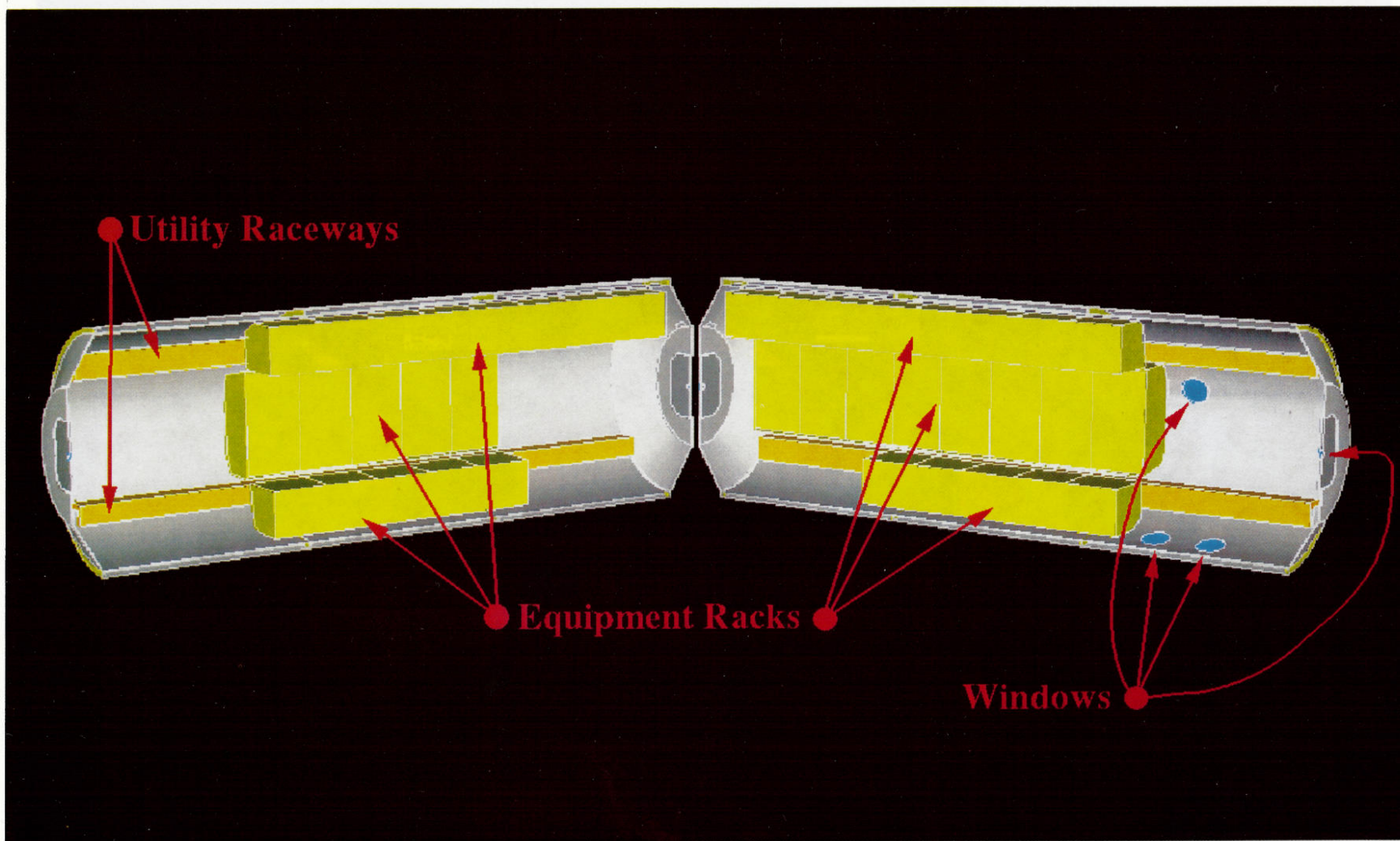
Figure 1. CAD-modeled split view of Space Station *Freedom* habitation module derivative.
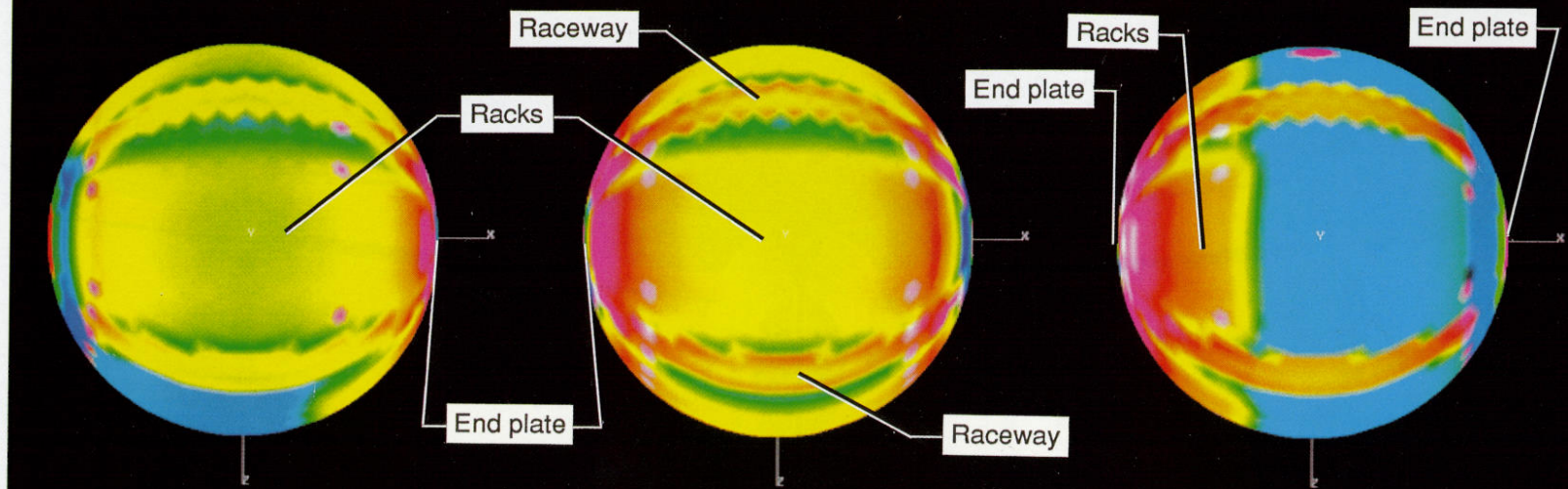
Figure 2. Directional thickness patterns for three interior points in CAD-modeled habitation module. Relative thickness increases as colors progress spectrally from blue to red.
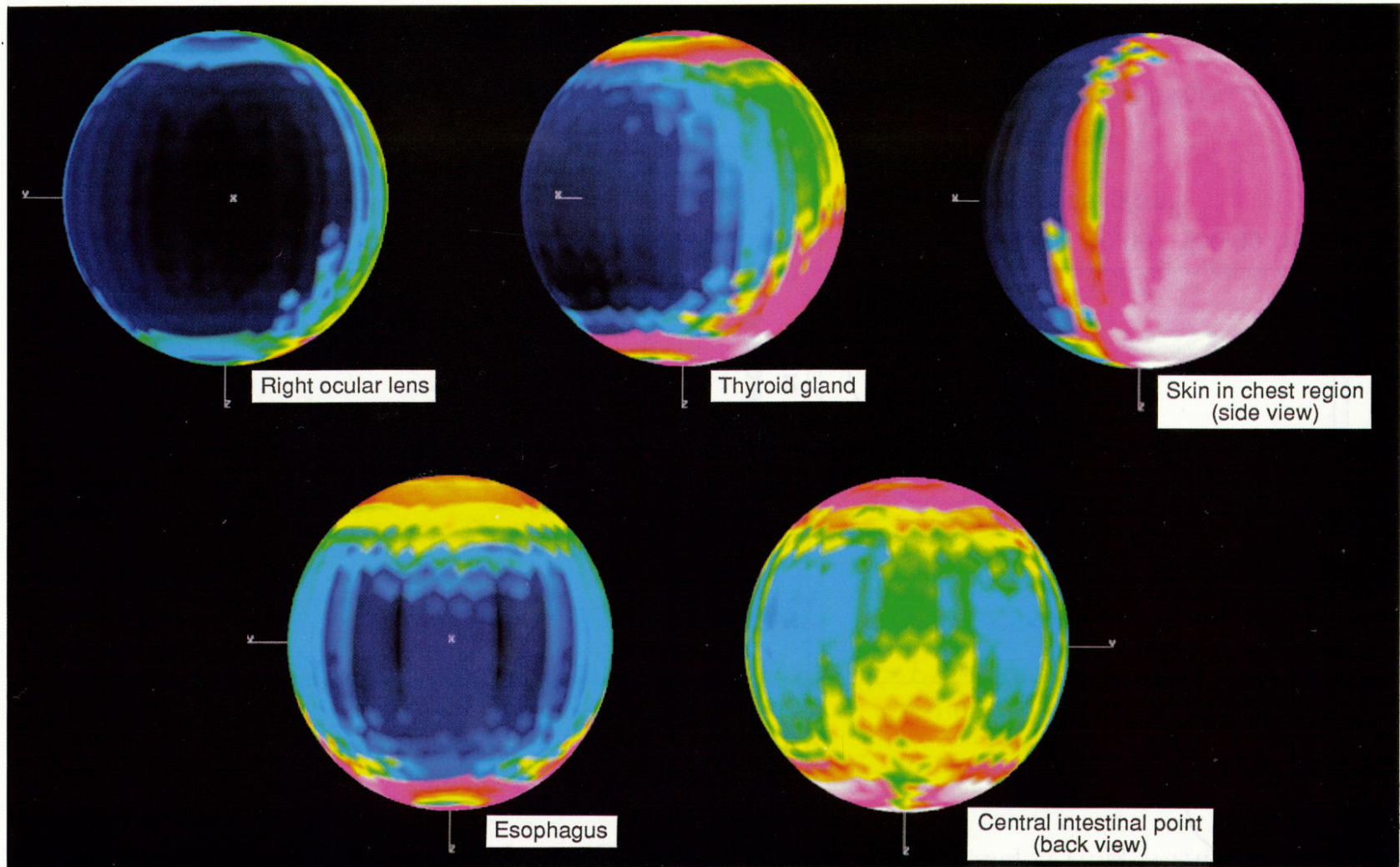
Figure 3. Directional thickness patterns for selected CAM model body target points. Relative thickness increases as colors progress spectrally from blue to red.
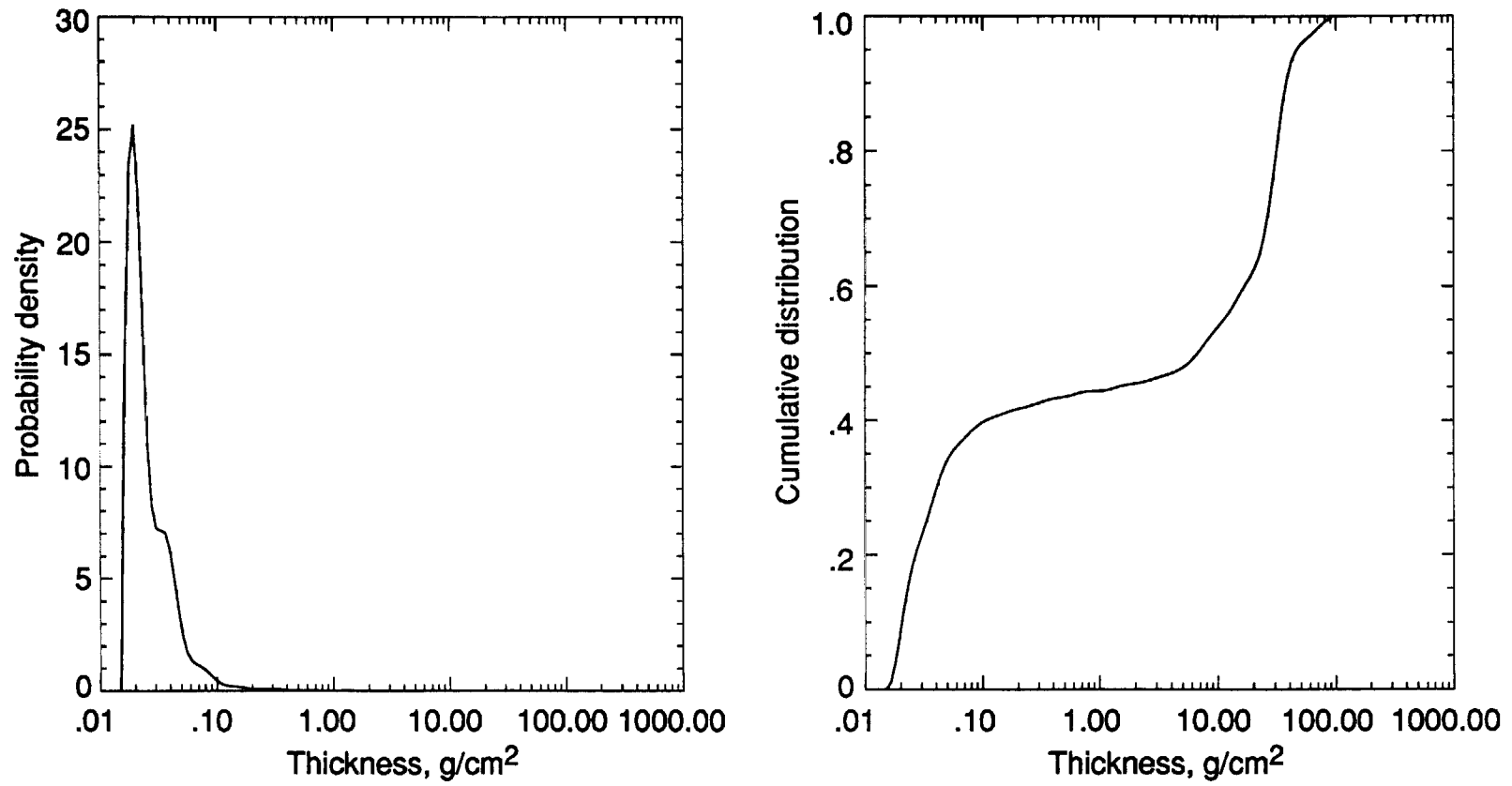
(a) Skin in chest region.

Figure 4. Thickness distribution functions obtained from CAM model for body target points.
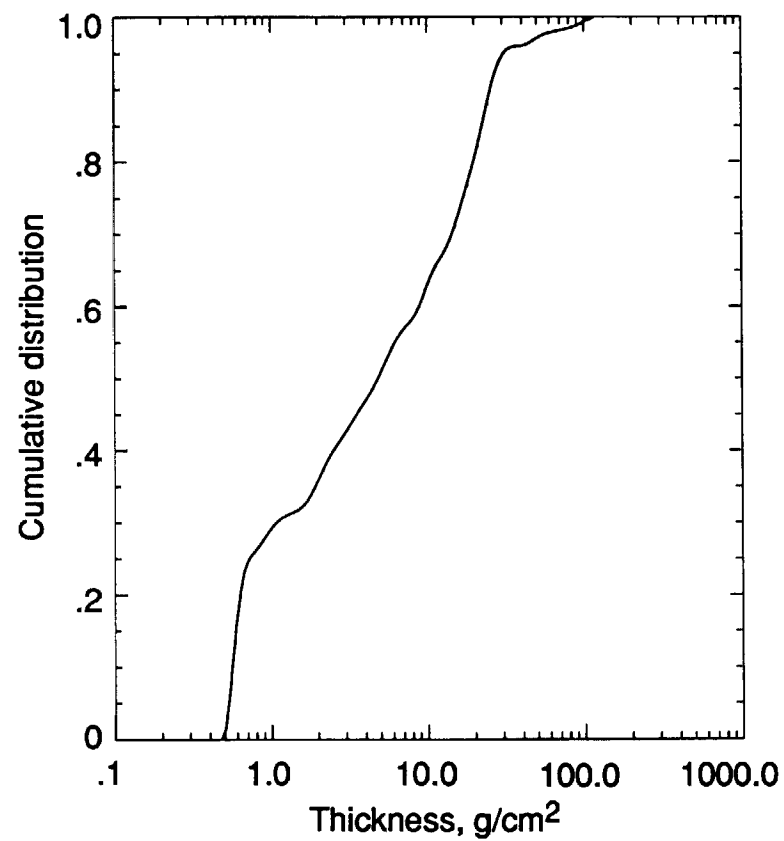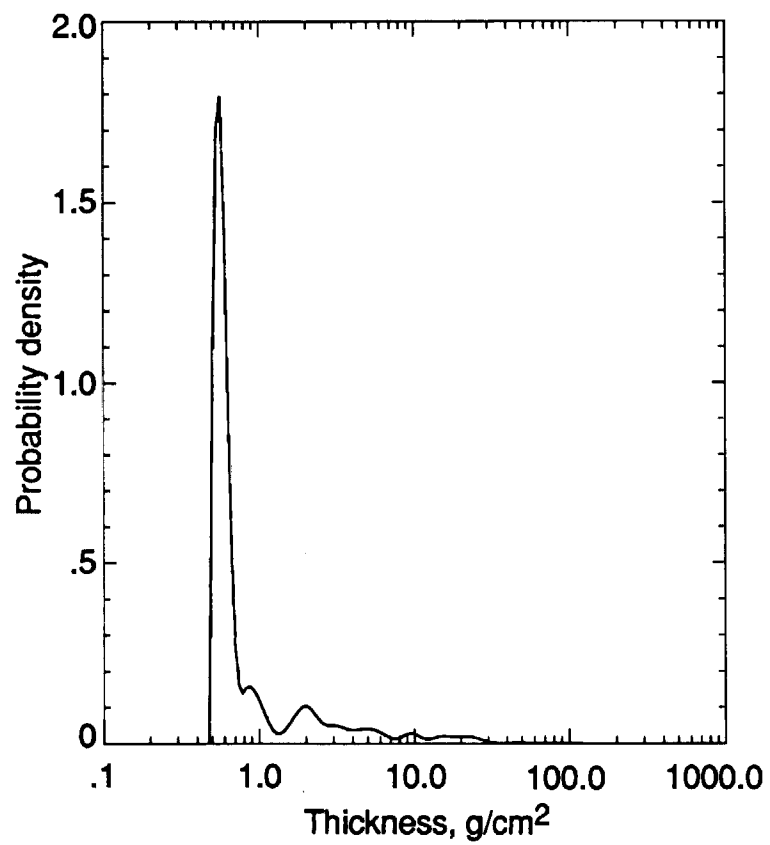
(b) Right ocular lens.

Figure 4. Continued.
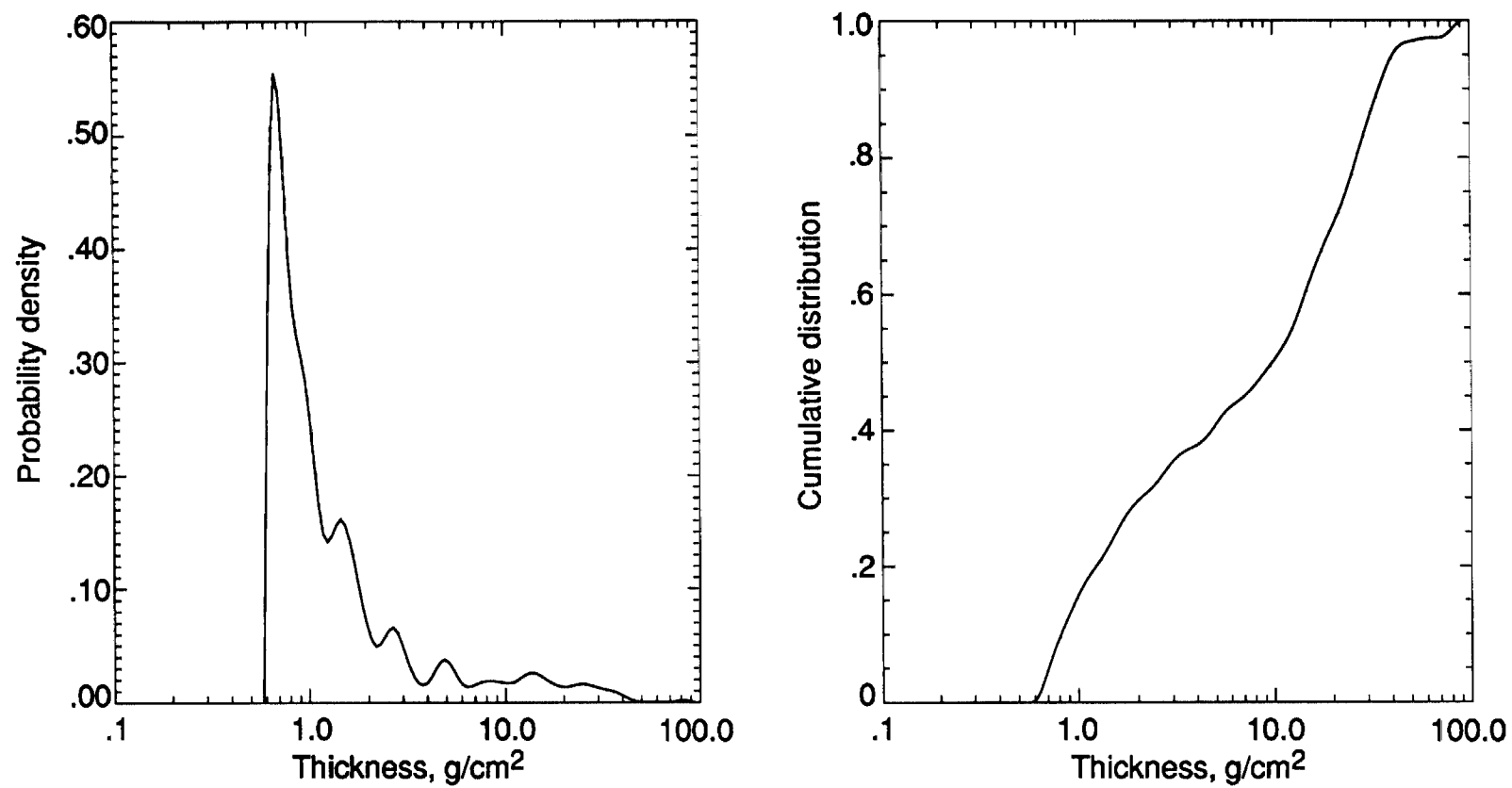
(c) Thyroid gland.

Figure 4. Continued.
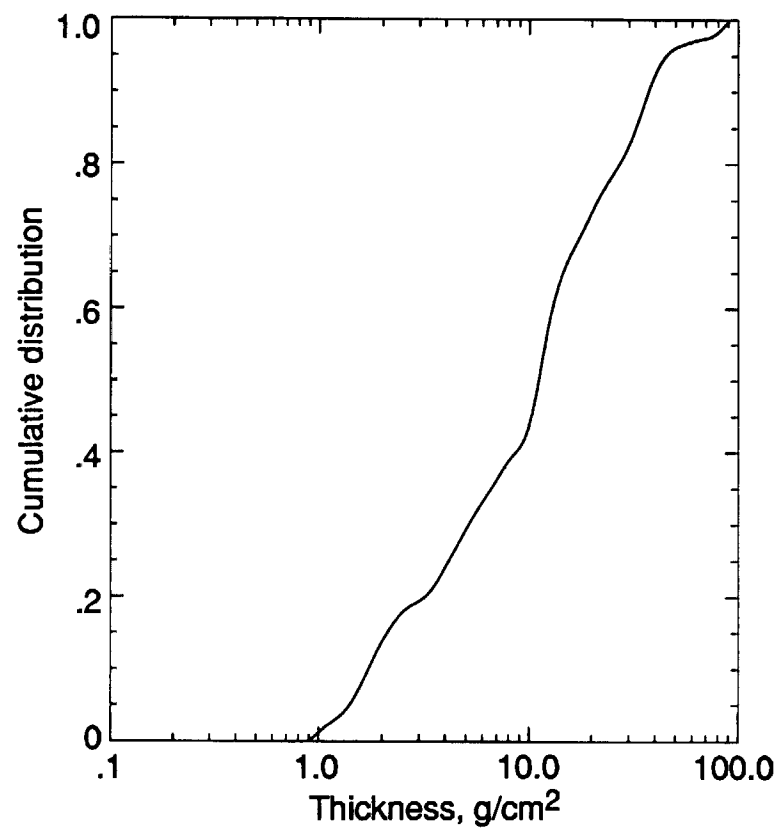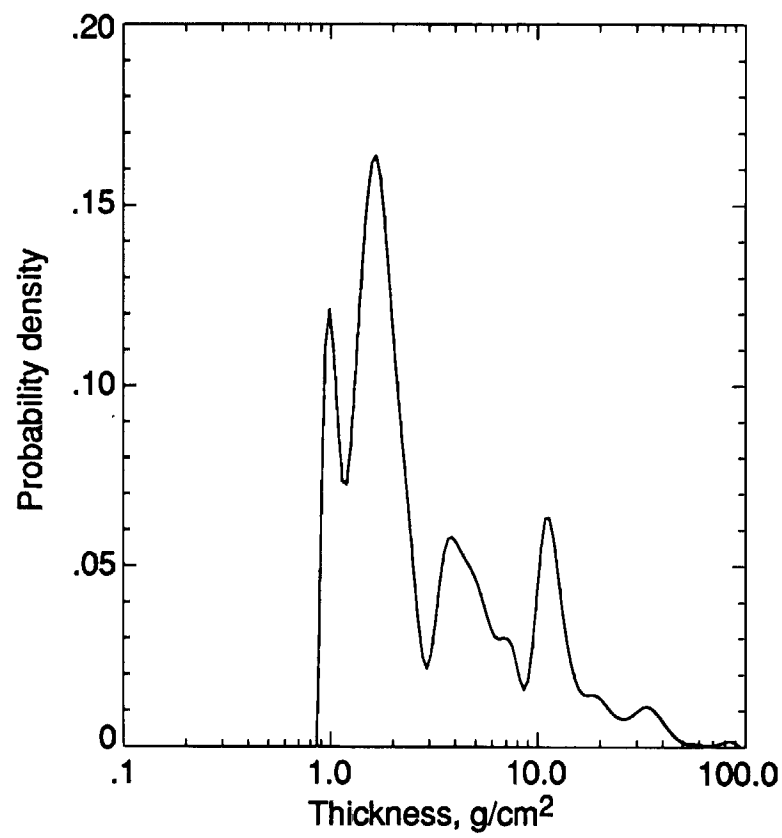
(d) Esophagus.

Figure 4. Continued.
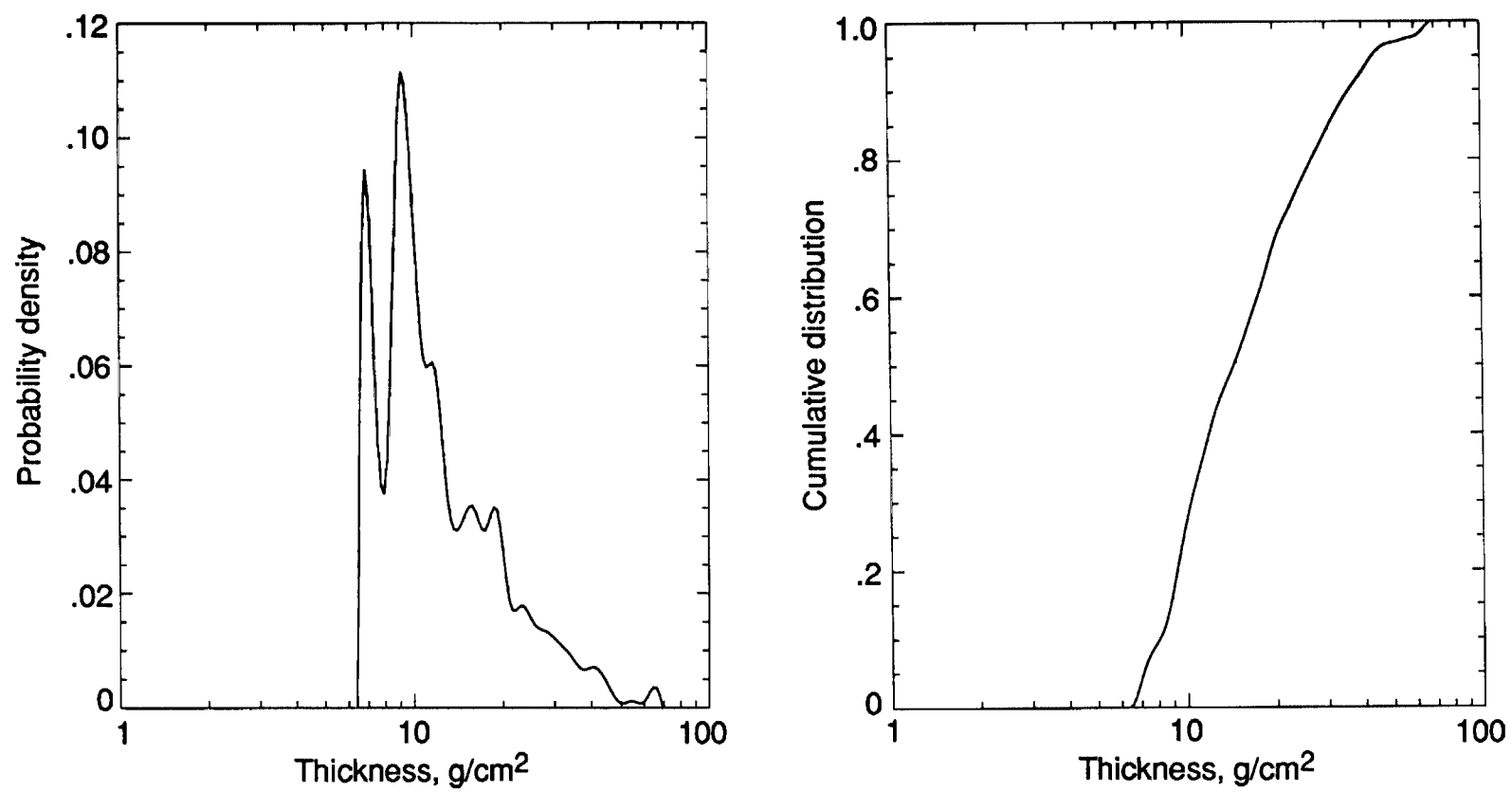
(e) Central intestinal point.

Figure 4. Concluded.
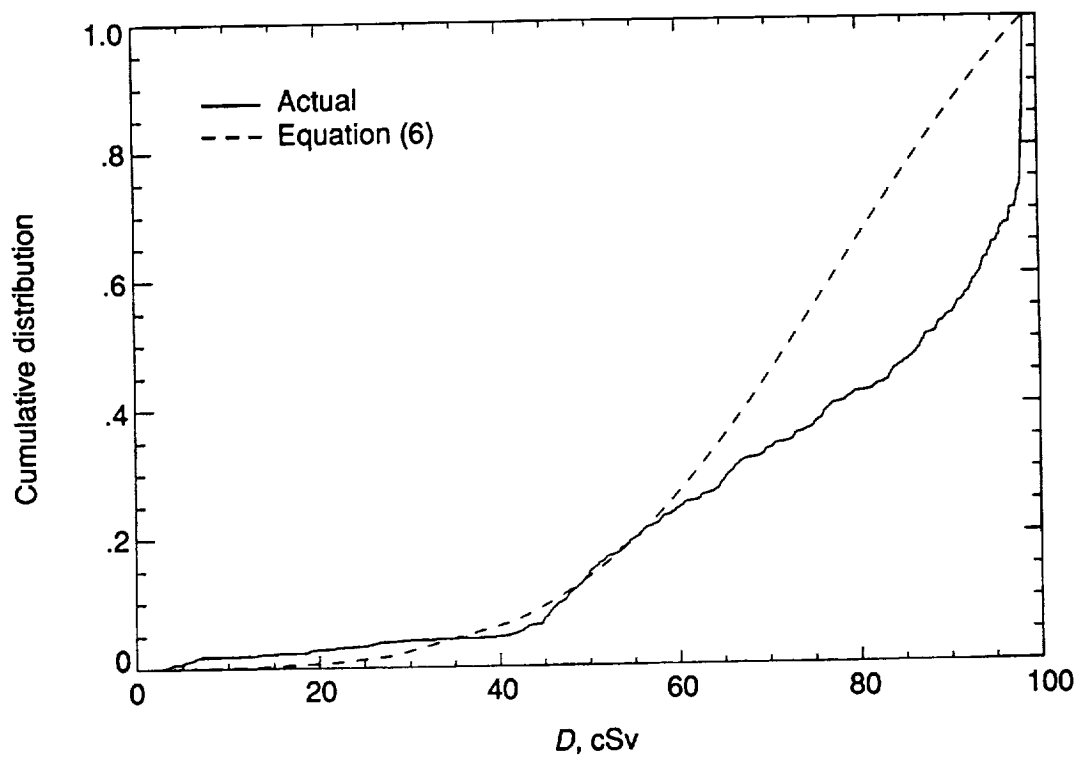
(a) Skin in chest region.
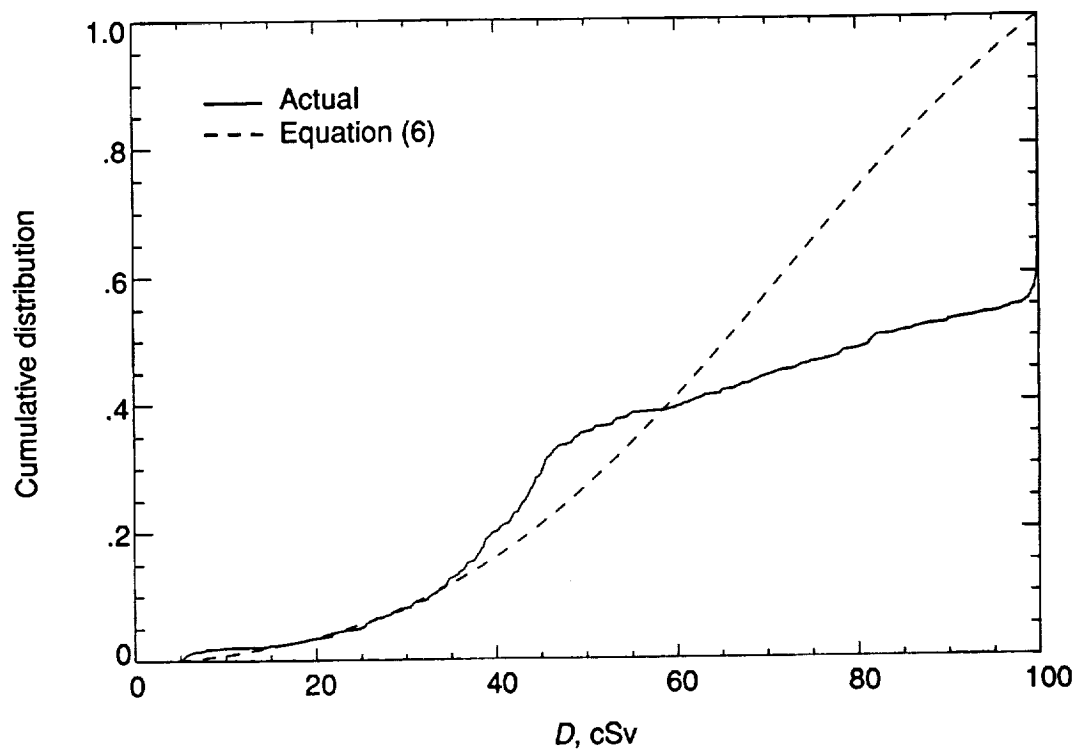
(b) Right ocular lens.

Figure 5. Cumulative dose distribution for monodirectional highly penetrating radiation in five body points. $\alpha = 0.04$ cm^2/g.
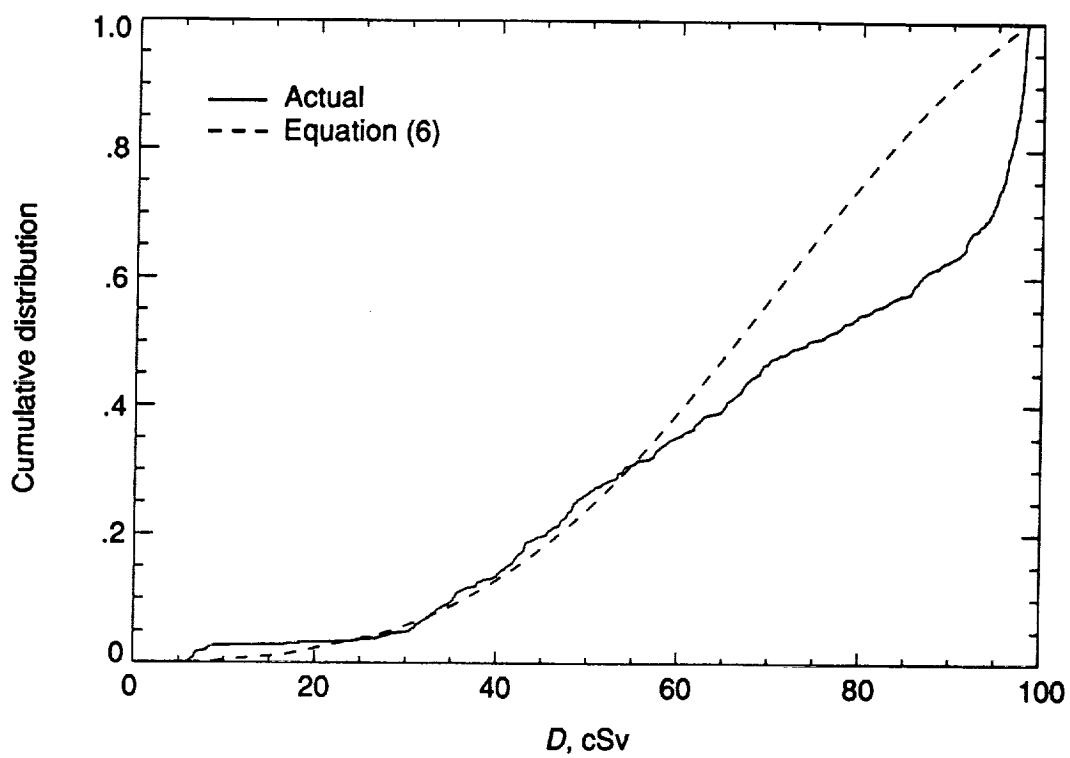
(c) Thyroid gland.
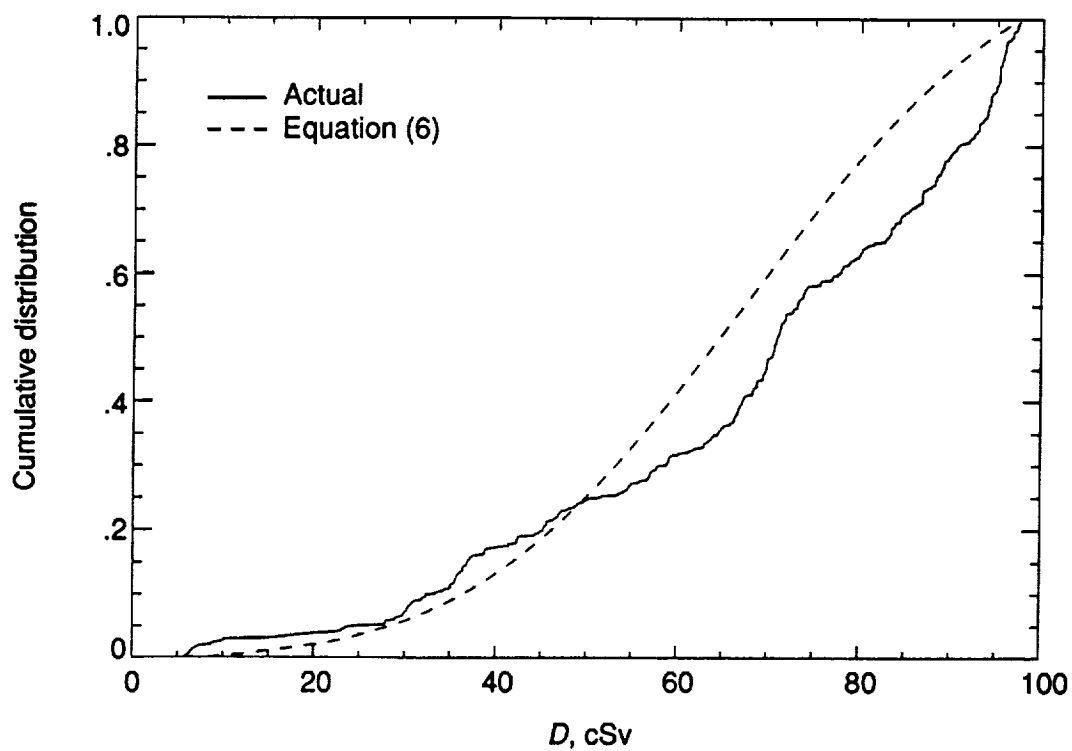
(d) Esophagus.

Figure 5. Continued.
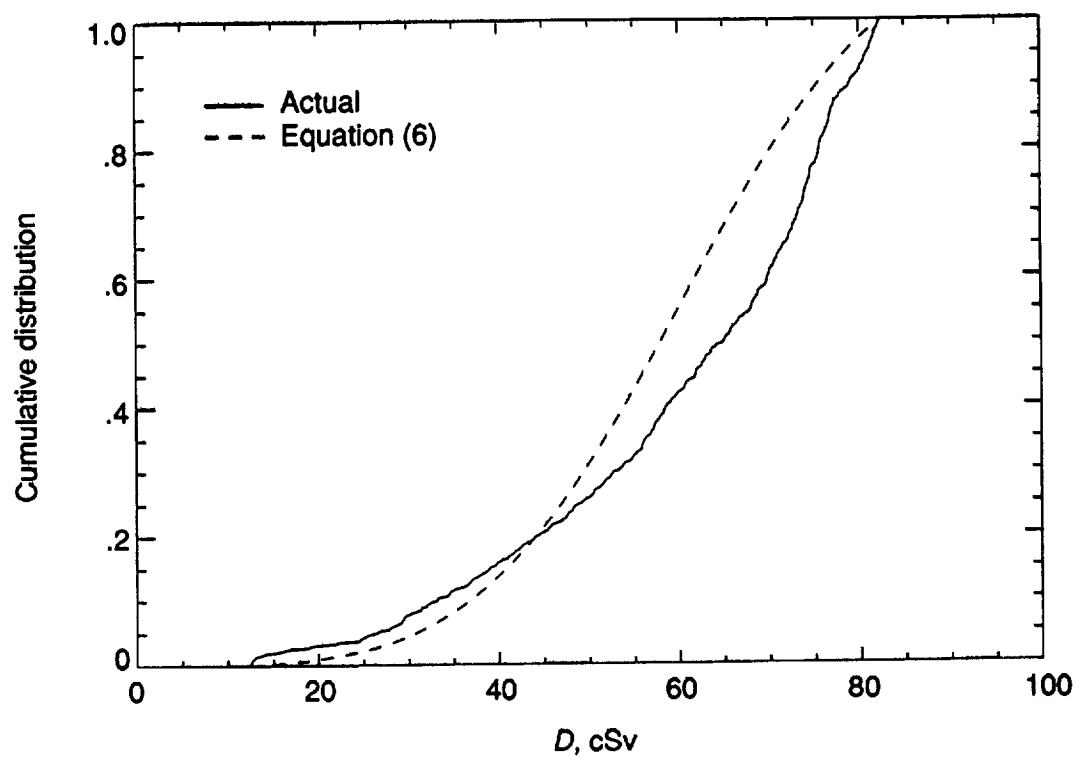
(e) Central intestinal point.

Figure 5. Concluded.
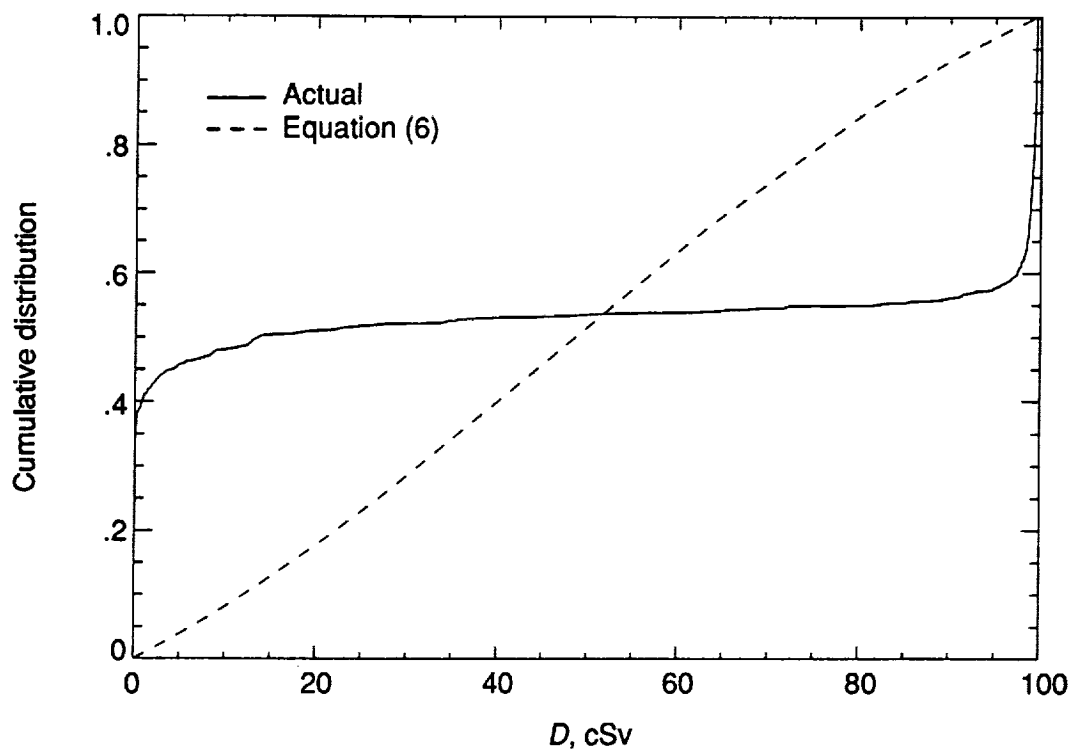
(a) Skin in chest region.
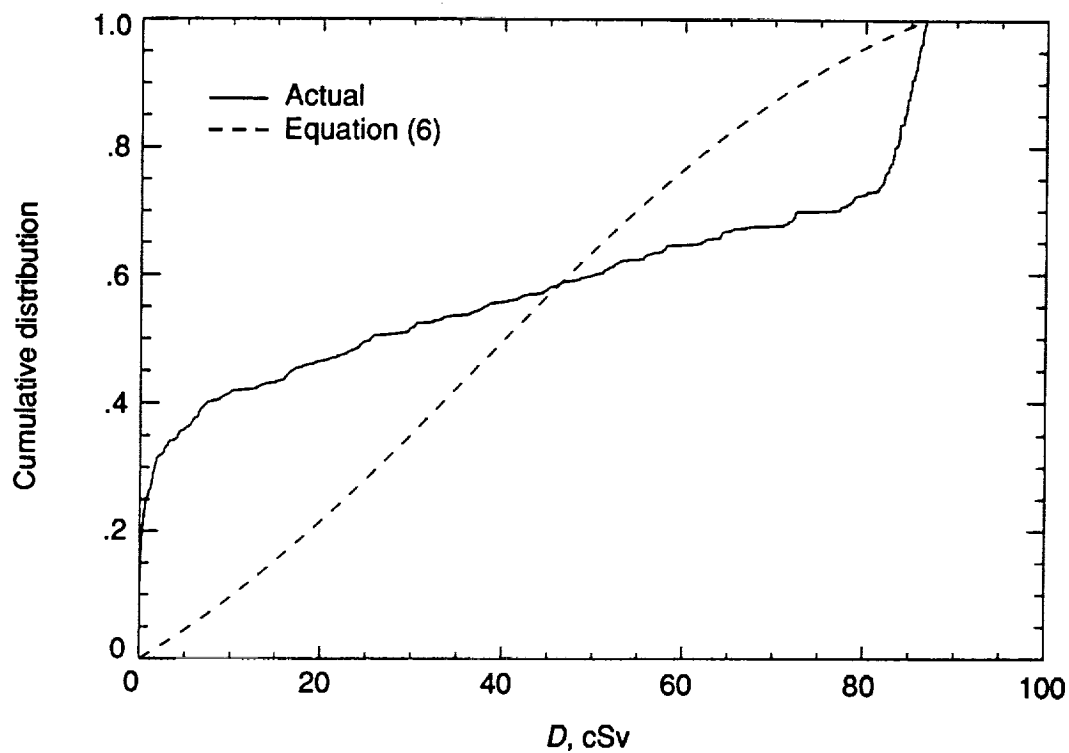
(b) Right ocular lens.

Figure 6. Cumulative dose distribution for monodirectional low penetration radiation in five body points. $\alpha = 0.4$ cm^2/g.
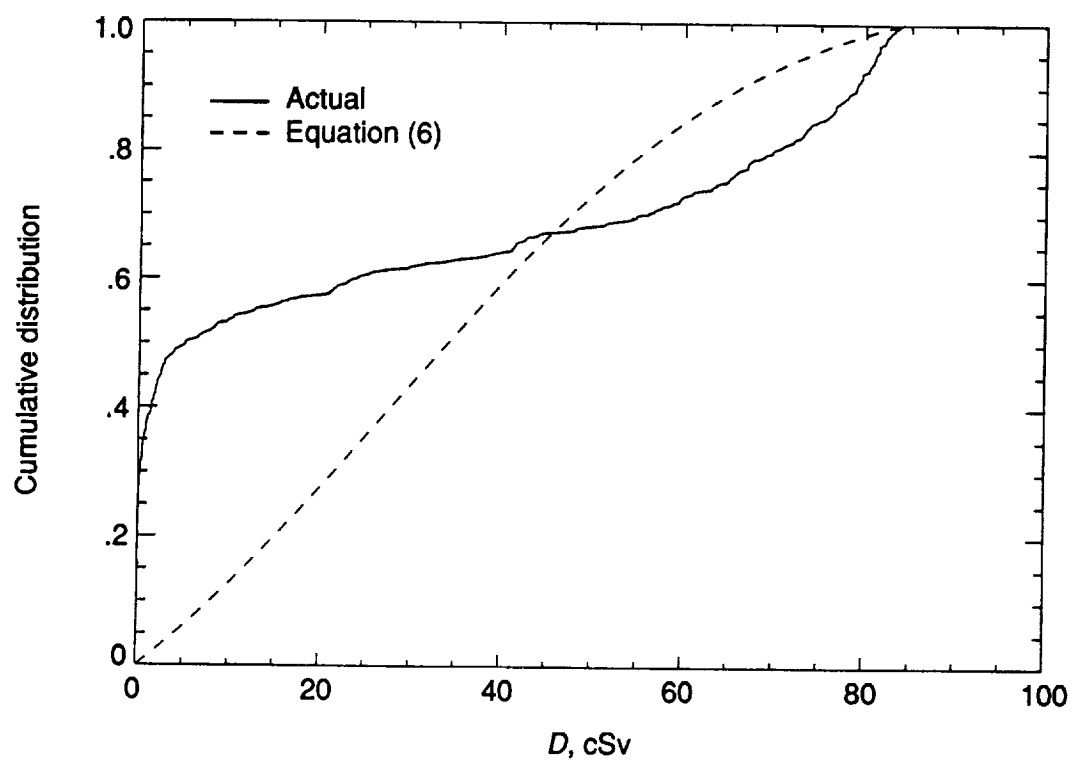
(c) Thyroid gland.
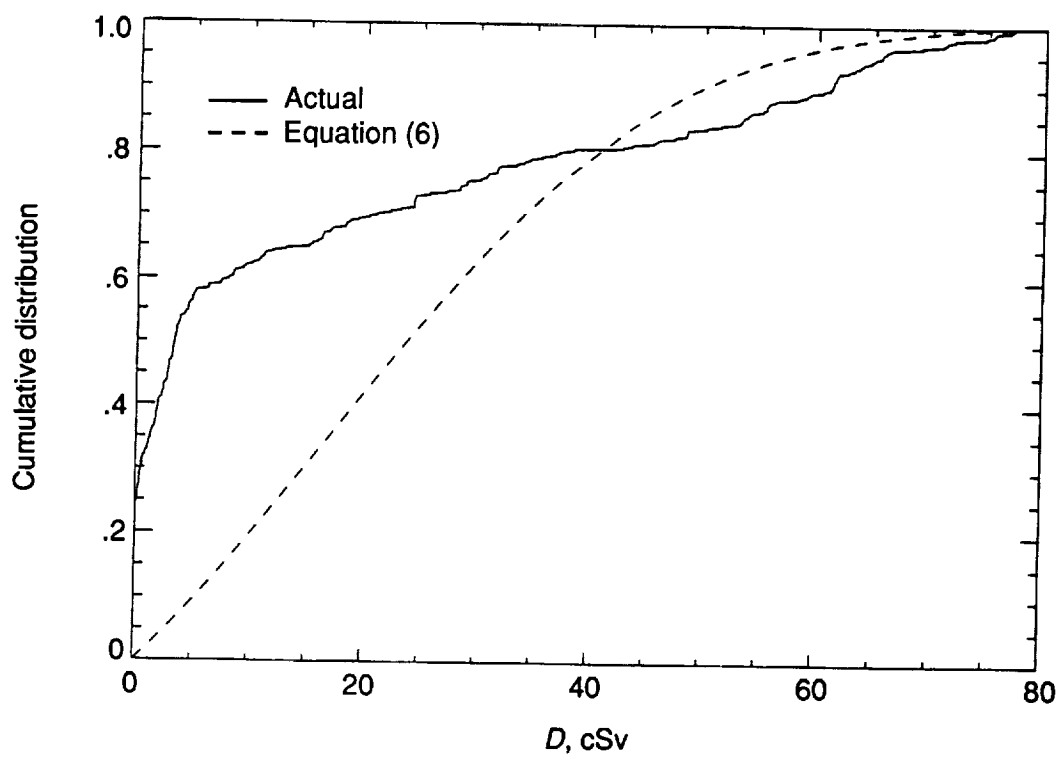
(d) Esophagus.

Figure 6. Continued.
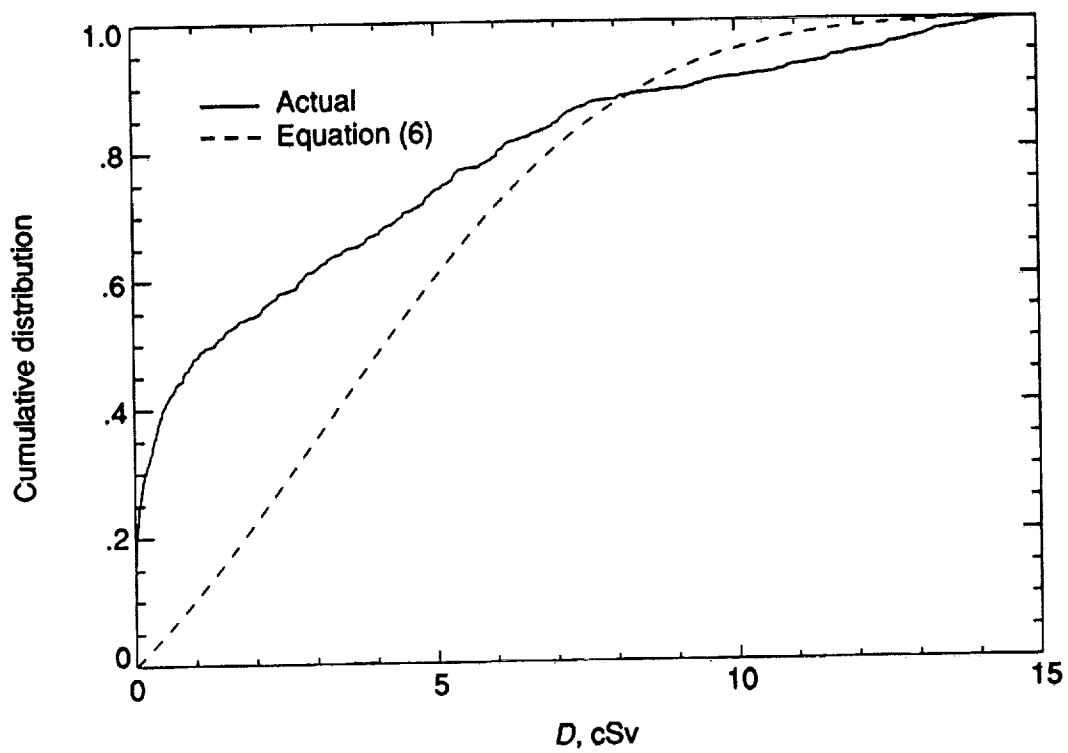
(e) Central intestinal point.

Figure 6. Concluded.
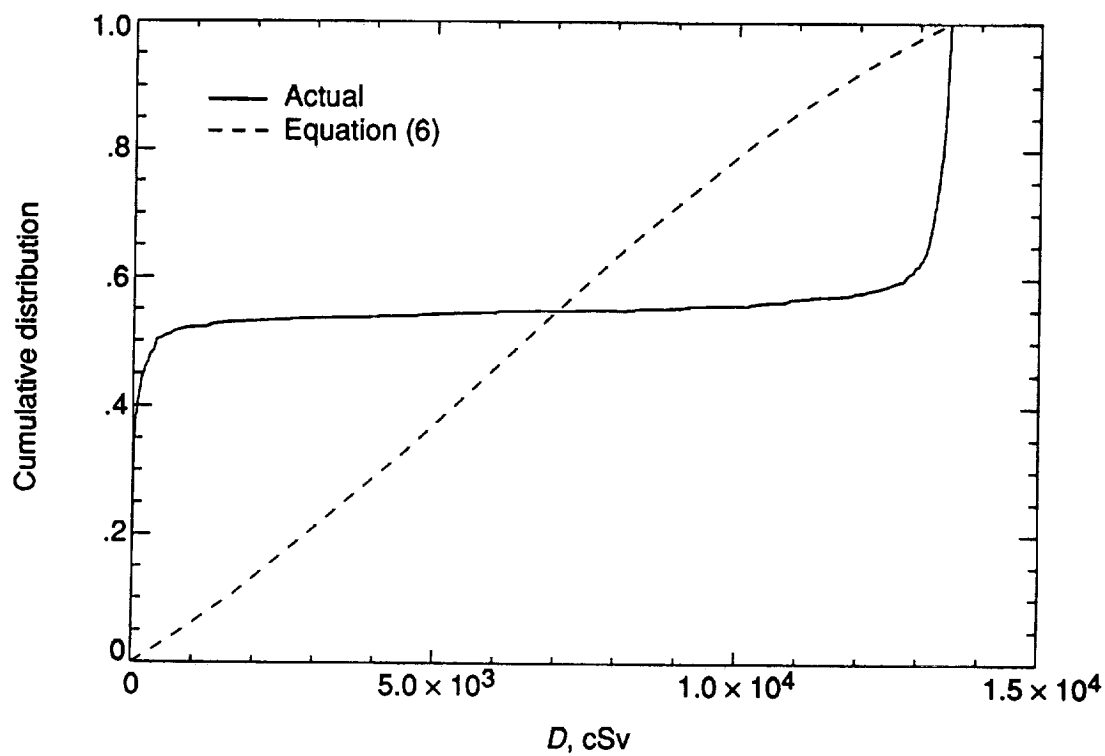
(a) Skin in chest region.
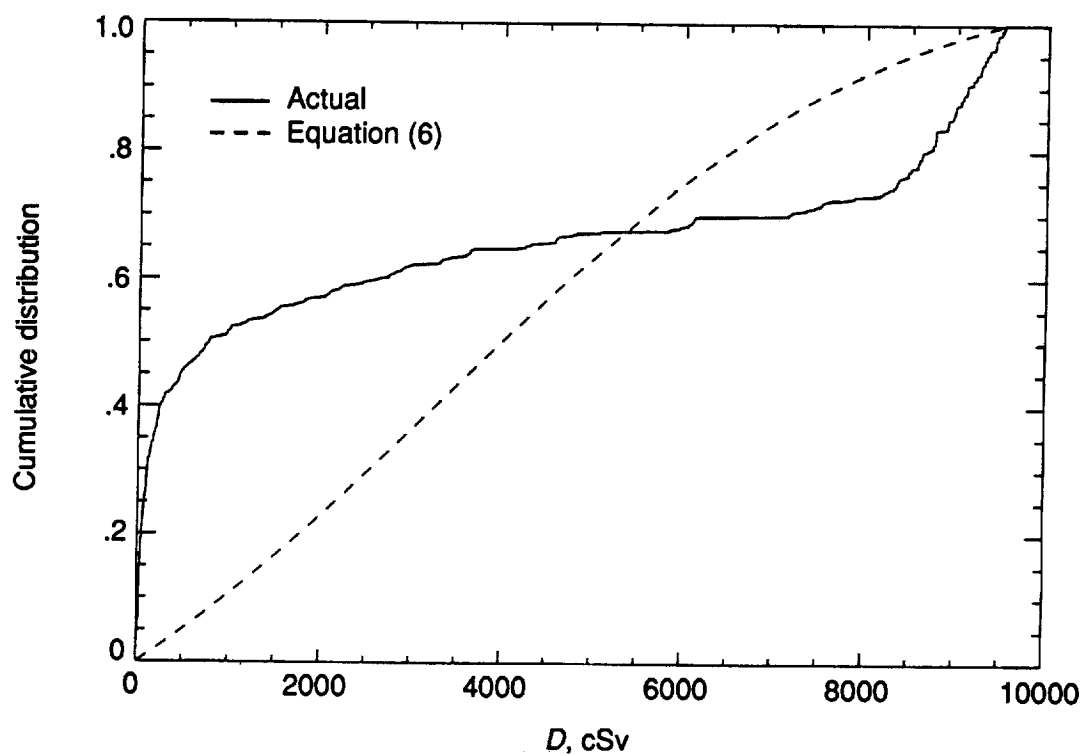
(b) Right ocular lens.

Figure 7. Cumulative dose distribution for assumed monodirectional October 1989 solar event in five body points.
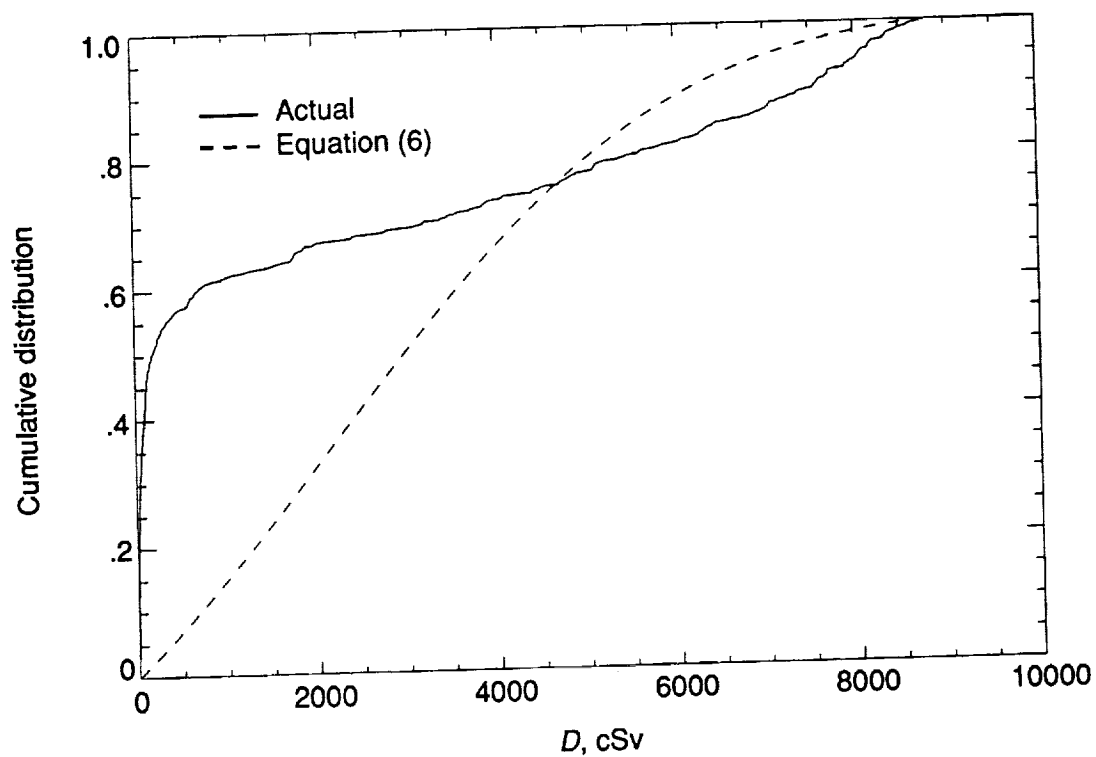
(c) Thyroid gland.
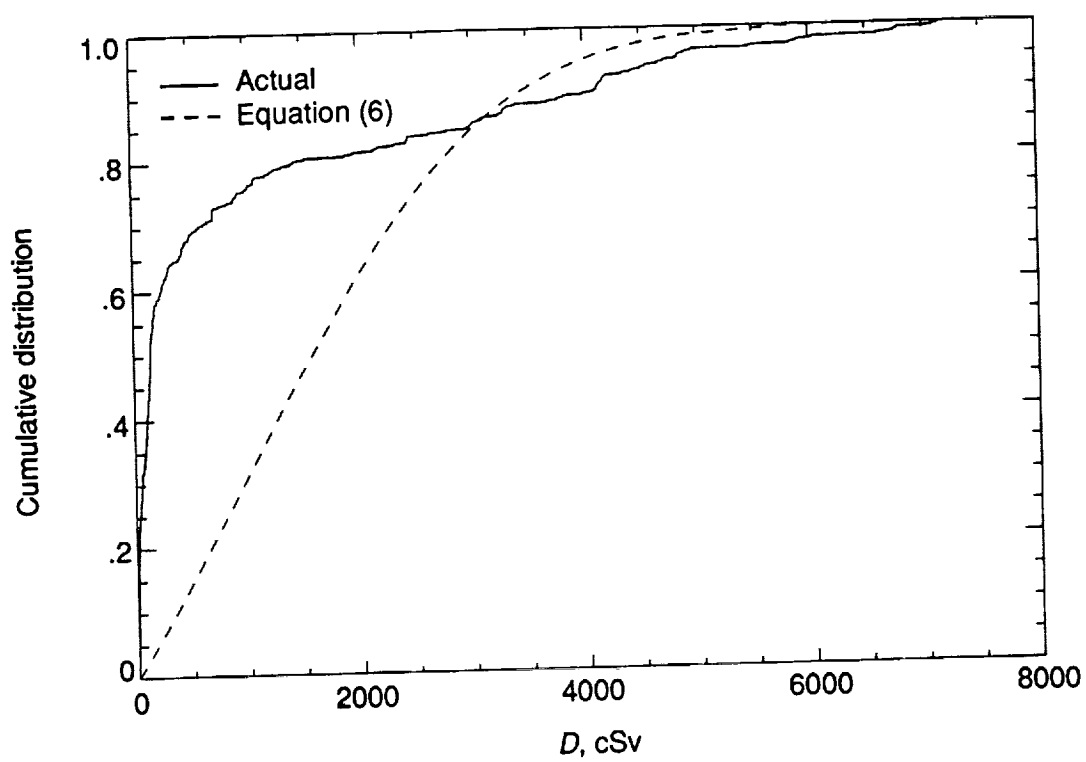
(d) Esophagus.

Figure 7. Continued.
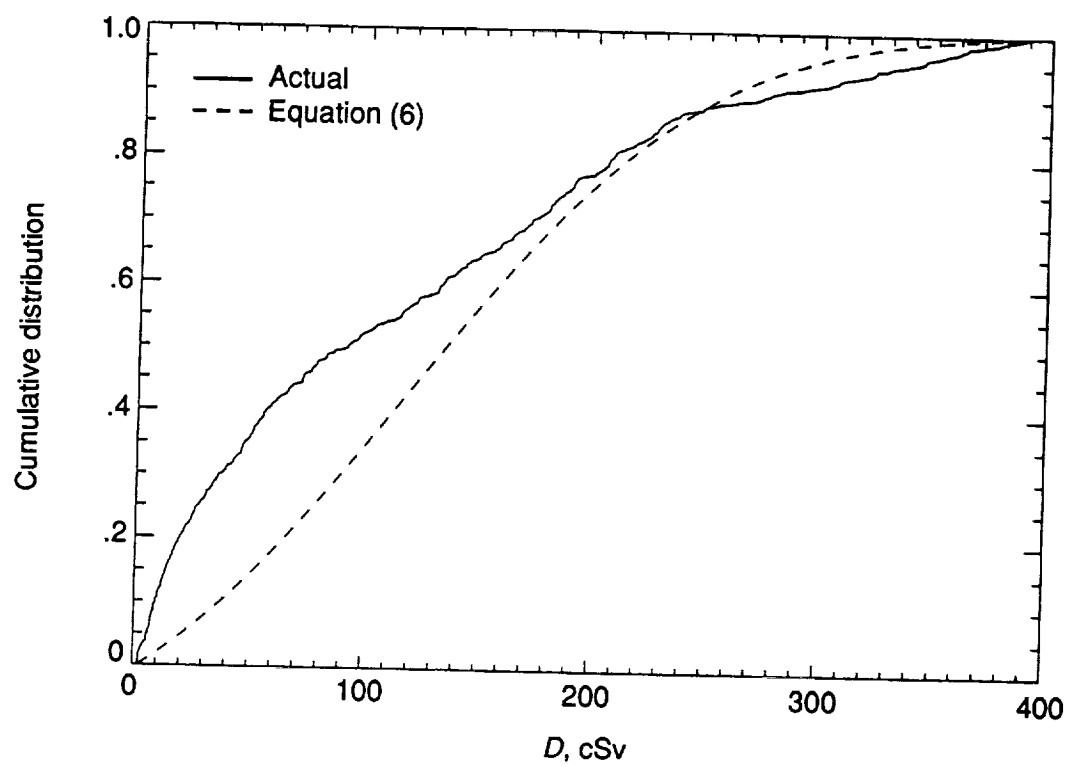
(e) Central intestinal point.

Figure 7. Concluded.
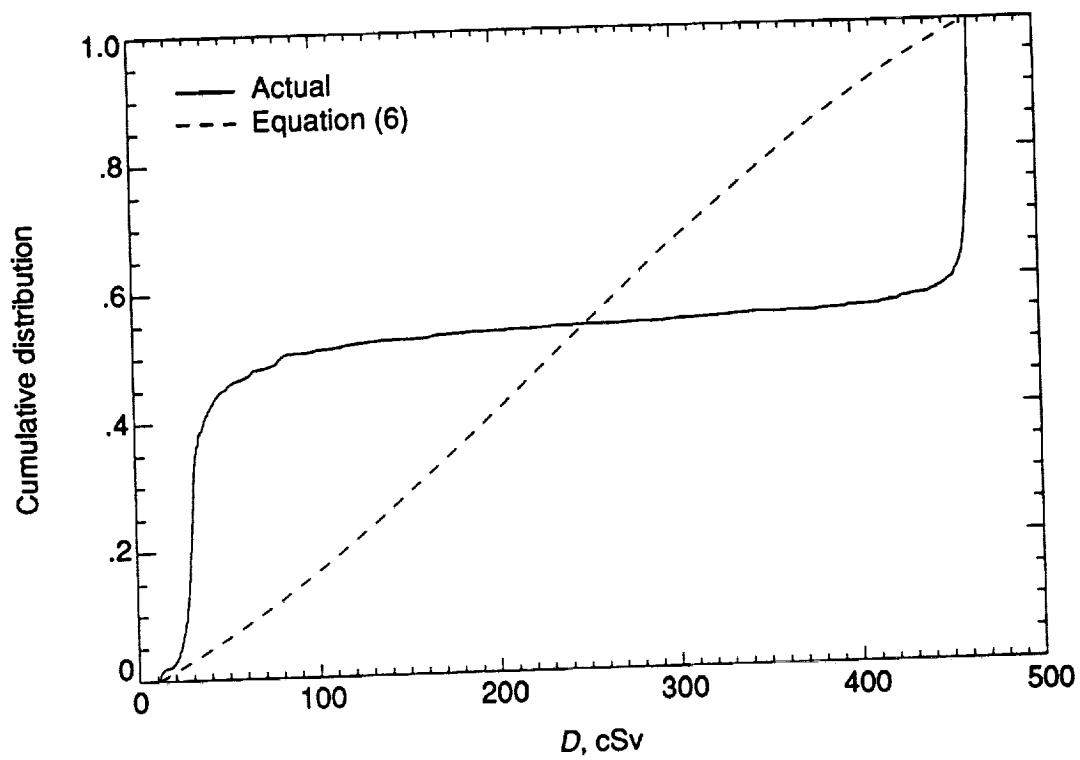
(a) Skin in chest region.
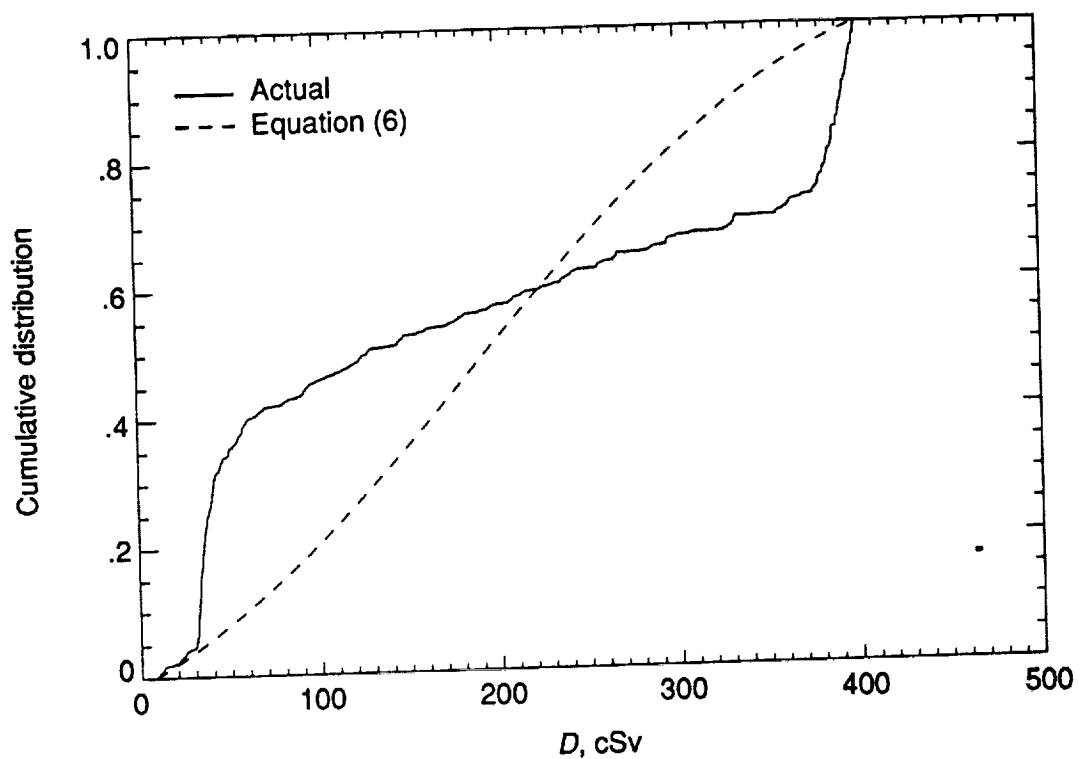
(b) Right ocular lens.

Figure 8. Cumulative dose distribution for assumed monodirectional February 1956 solar event in five body points.
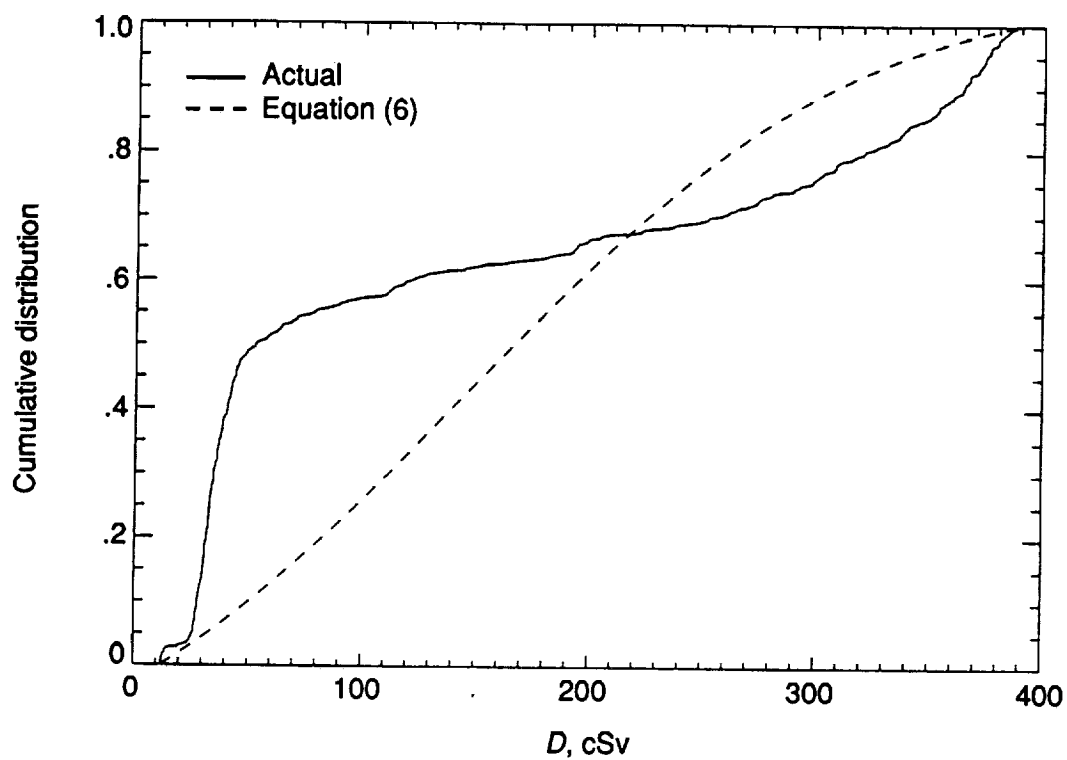
(c) Thyroid gland.
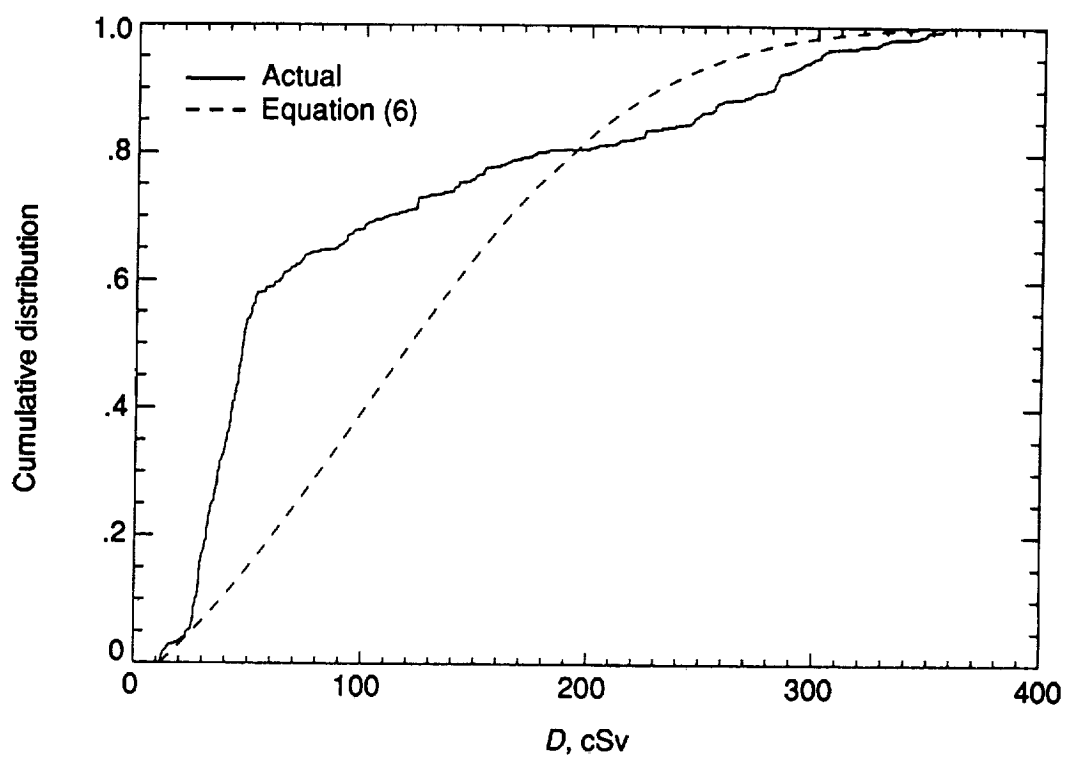
(d) Esophagus.

Figure 8. Continued.
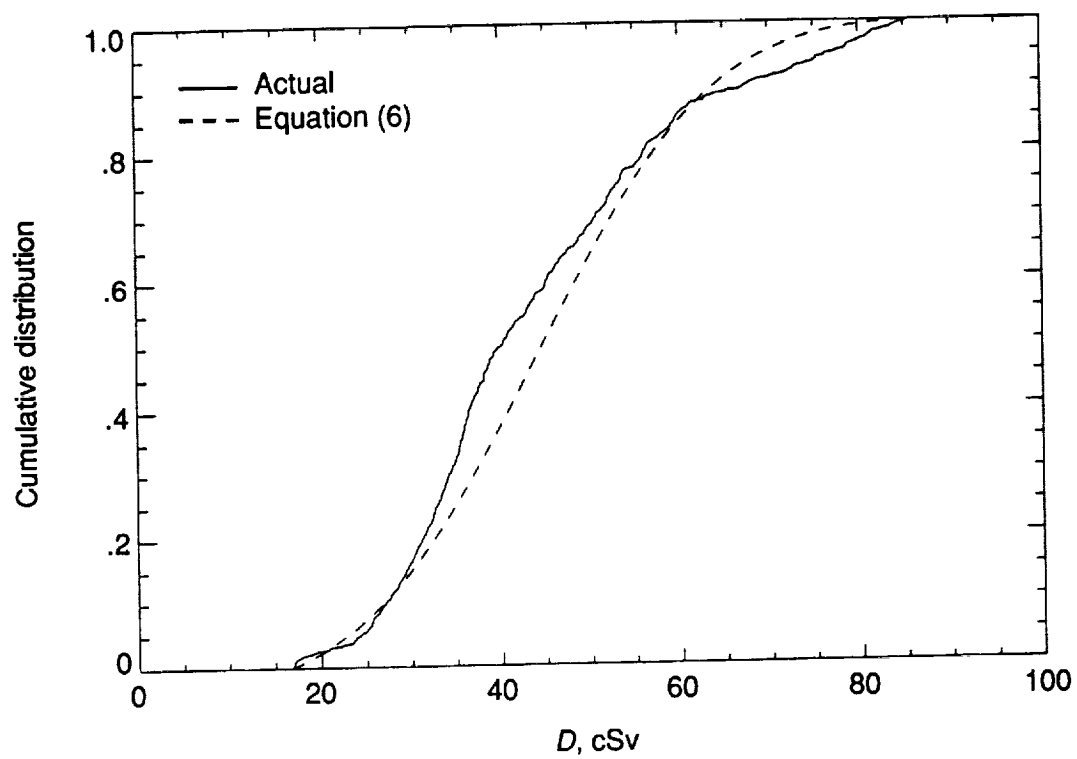
(e) Central intestinal point.

Figure 8. Concluded.
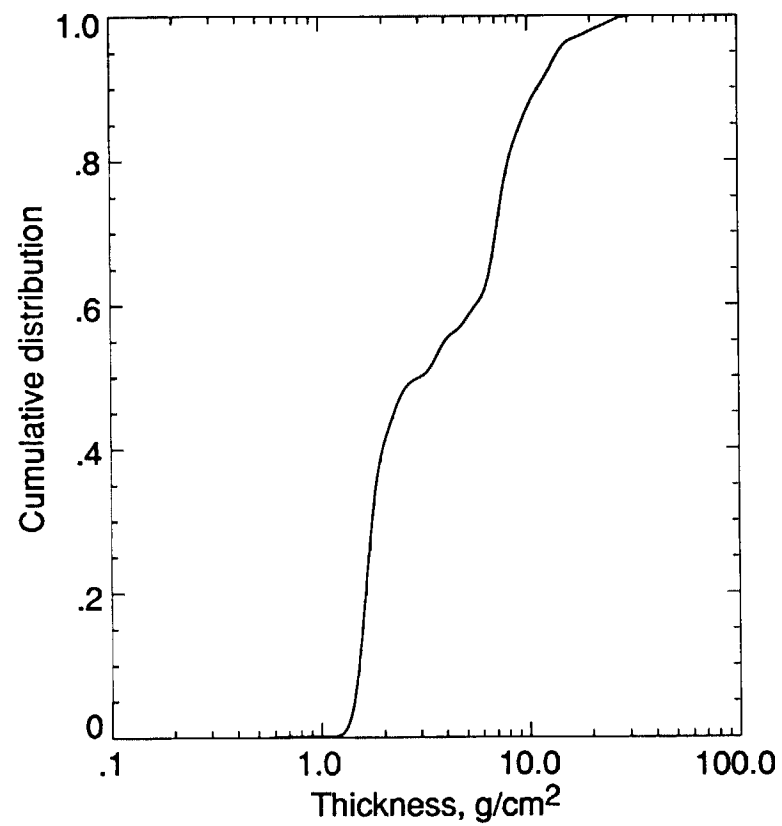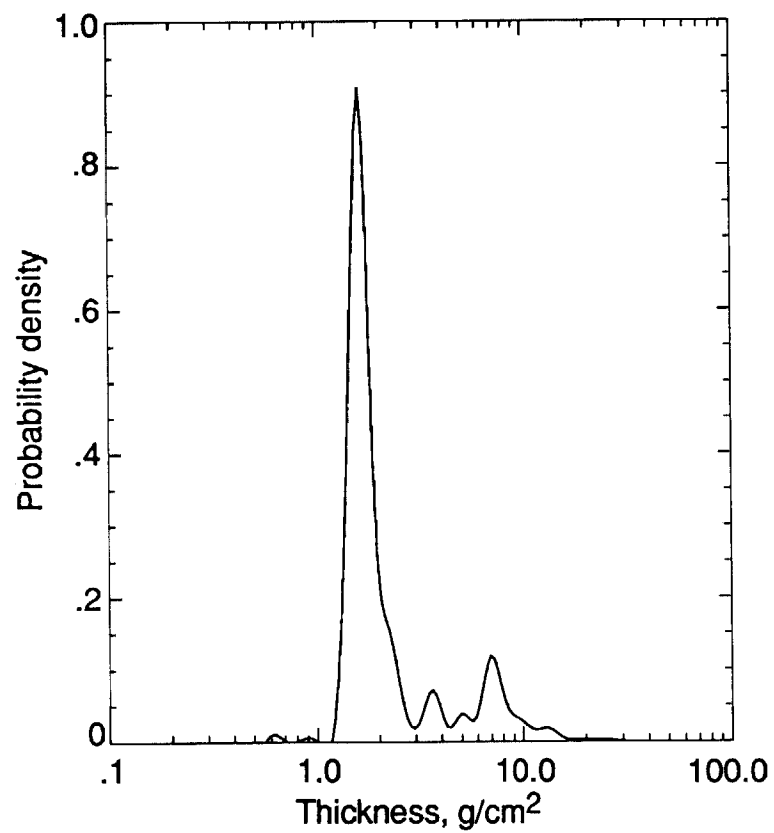
(a) Point A.

Figure 9. Thickness distribution functions obtained from CAD-modeled habitation module.
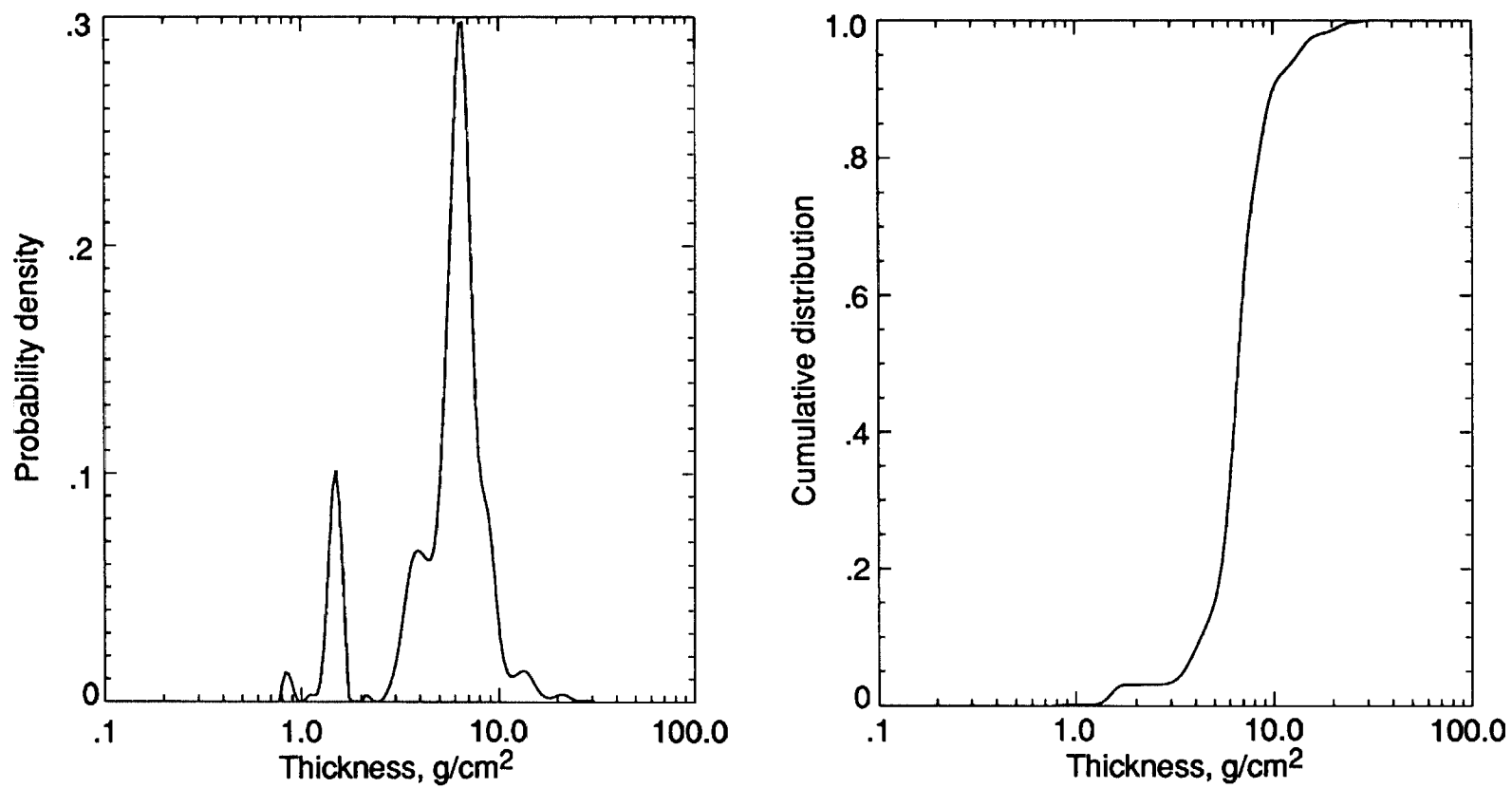
(b) Point B.

Figure 9. Continued.
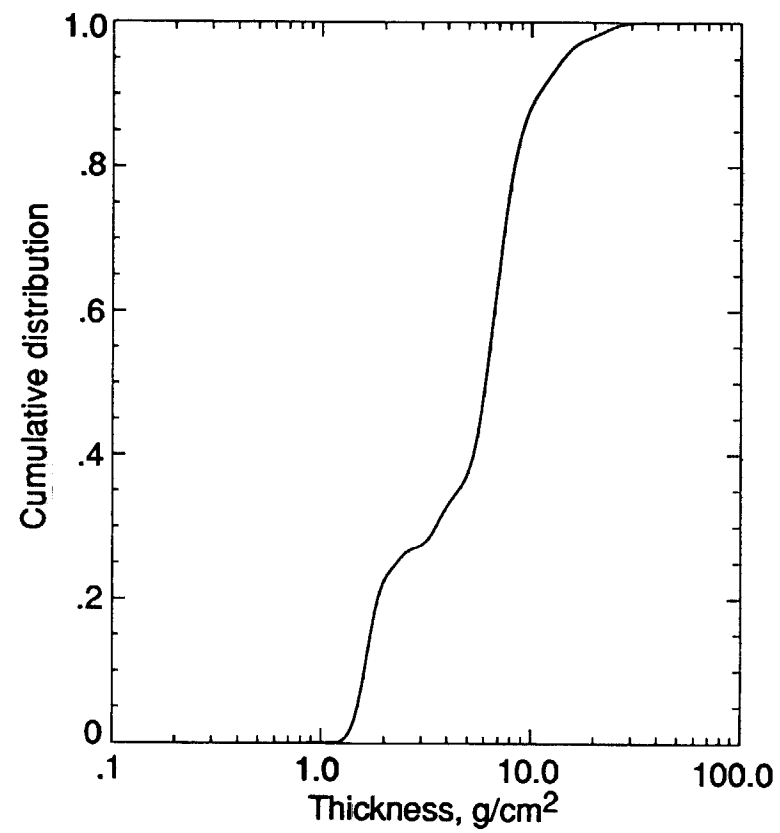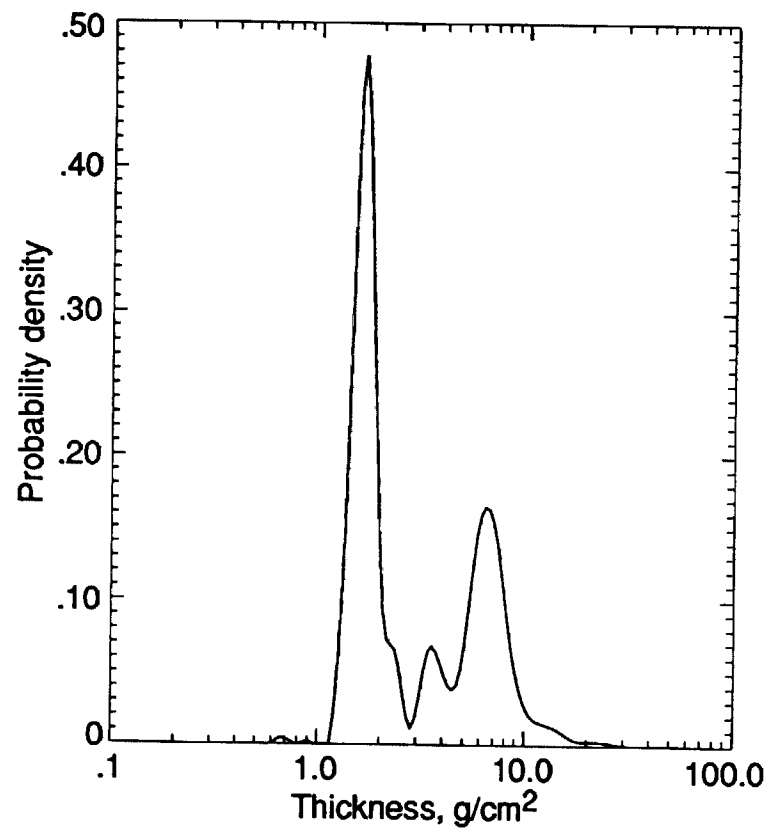
(c) Point C.

Figure 9. Concluded.
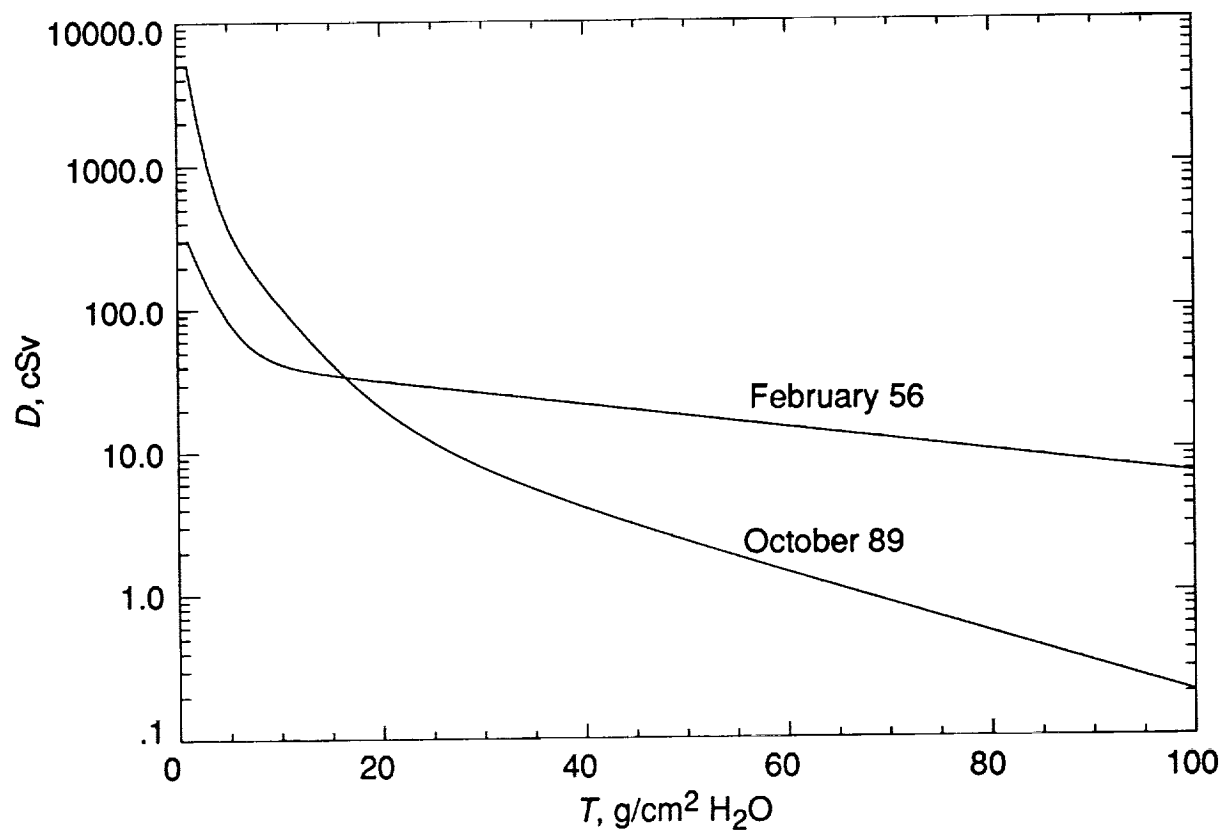
Figure 10. Computed dose-versus-depth functions for observed proton flare spectra.
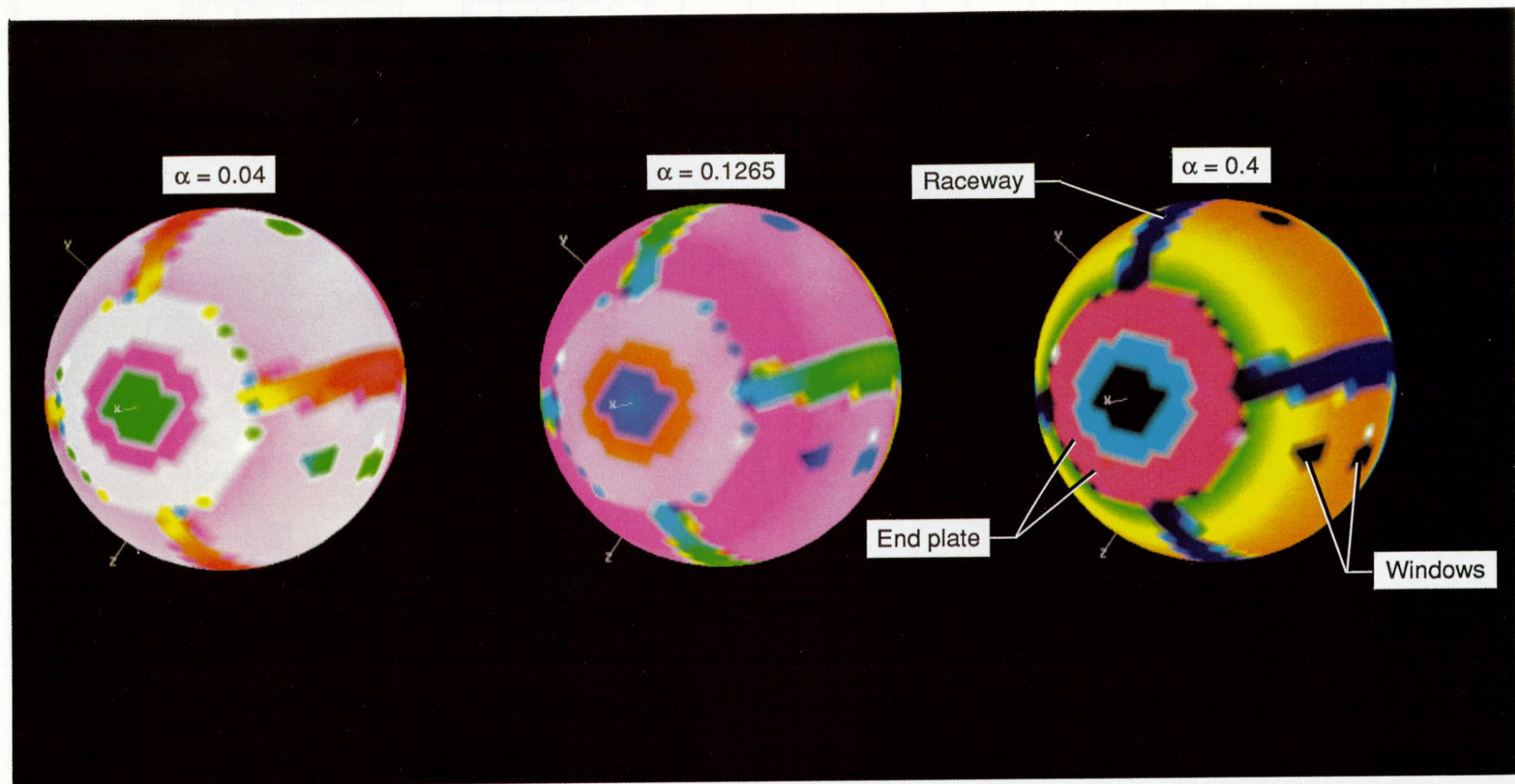
Figure 11. Directional dose patterns at habitation module point A for idealized dose-versus-depth functions with selected attenuation coefficients. Relative dose increases as colors progress spectrally from blue to red.
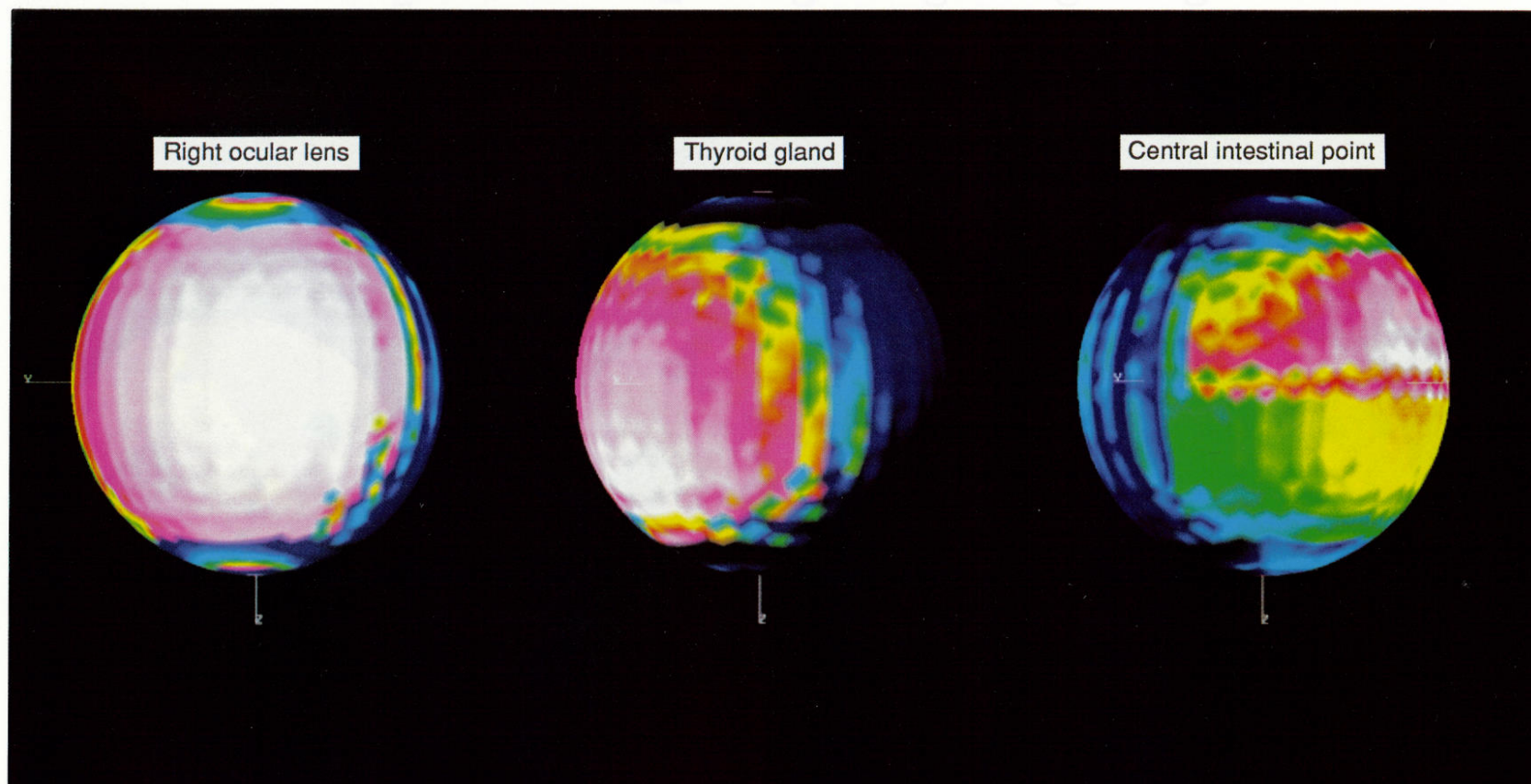
Figure 12. Dose patterns at CAM model body points for 1989 proton flare dose-versus-depth function. Relative dose increases as colors progress spectrally from blue to red.
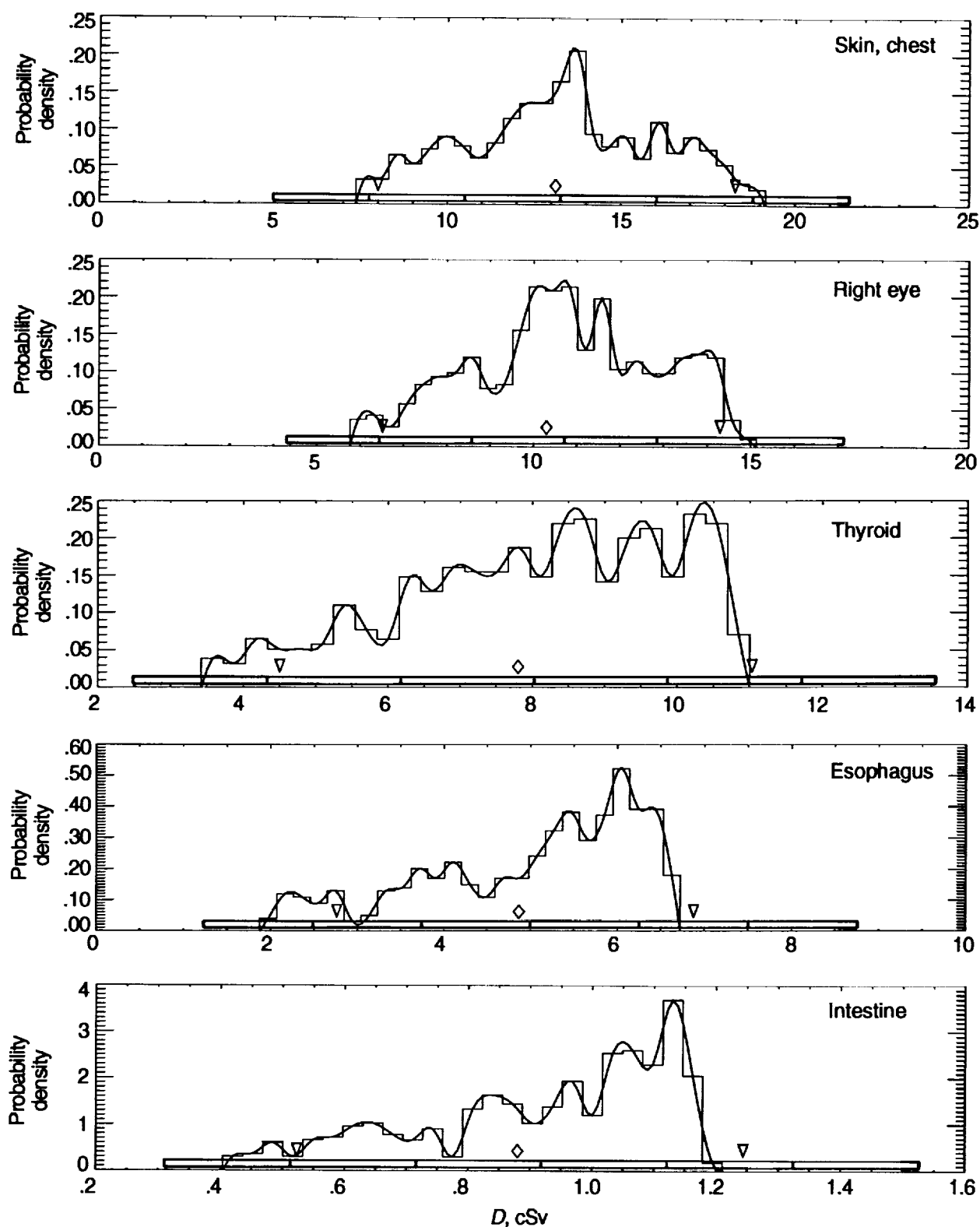
(a) Highly attenuating dose-versus-depth function. $\alpha = 0.4$.

Figure 13. Dose probability density functions for body target points randomly oriented within simulated habitat at point A.
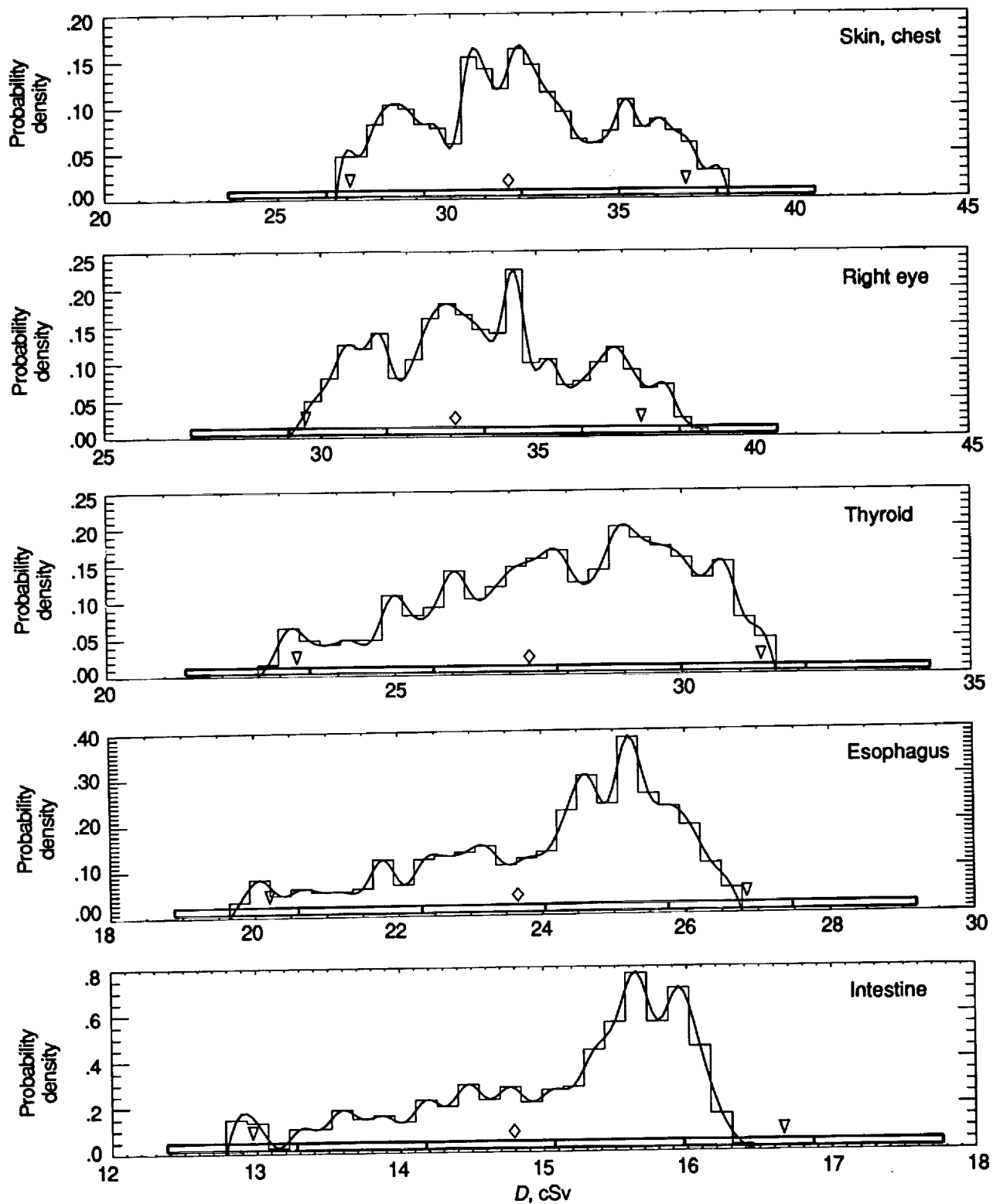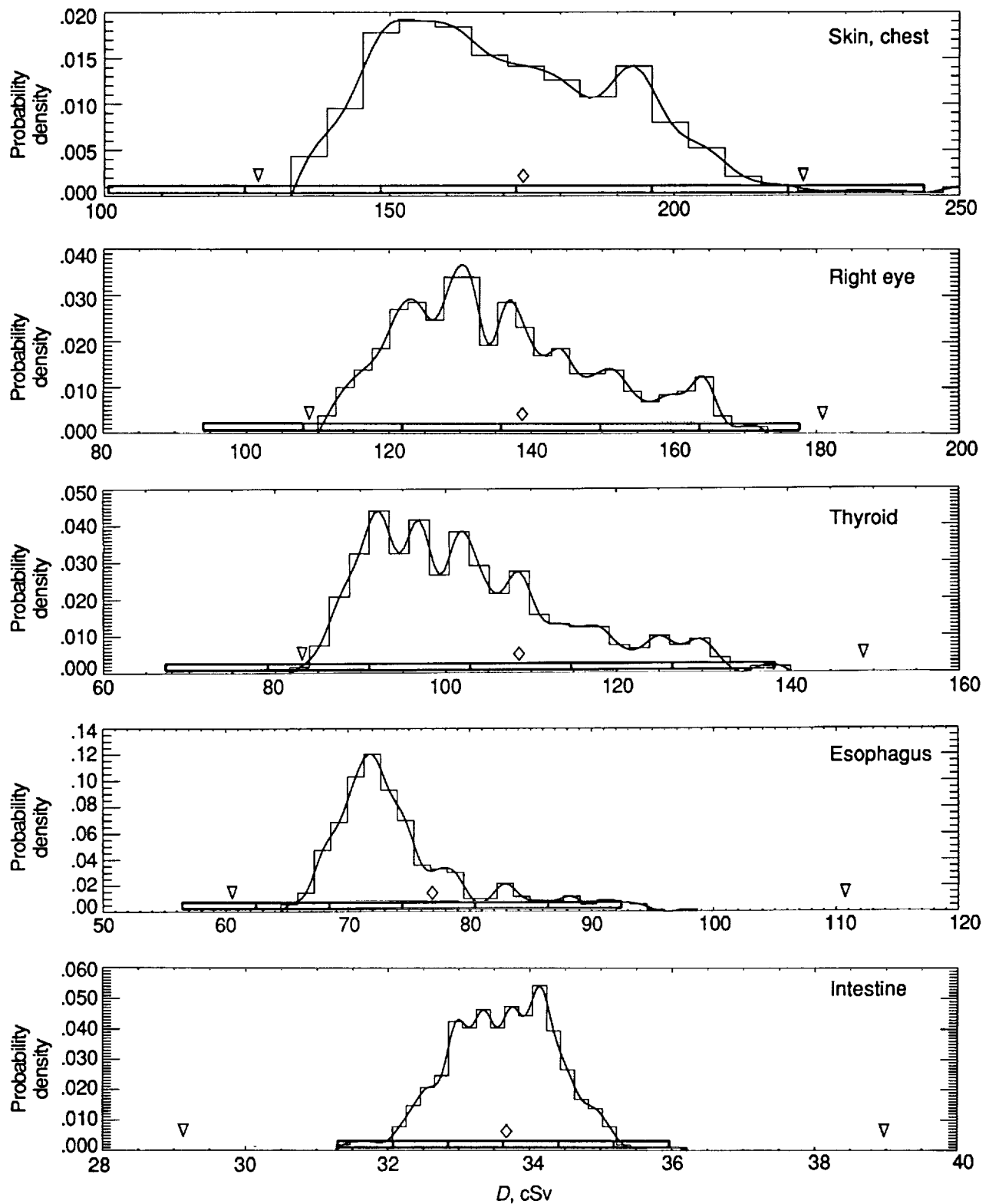
(b) Moderately attenuating dose-versus-depth function. $\alpha = 0.1265$.
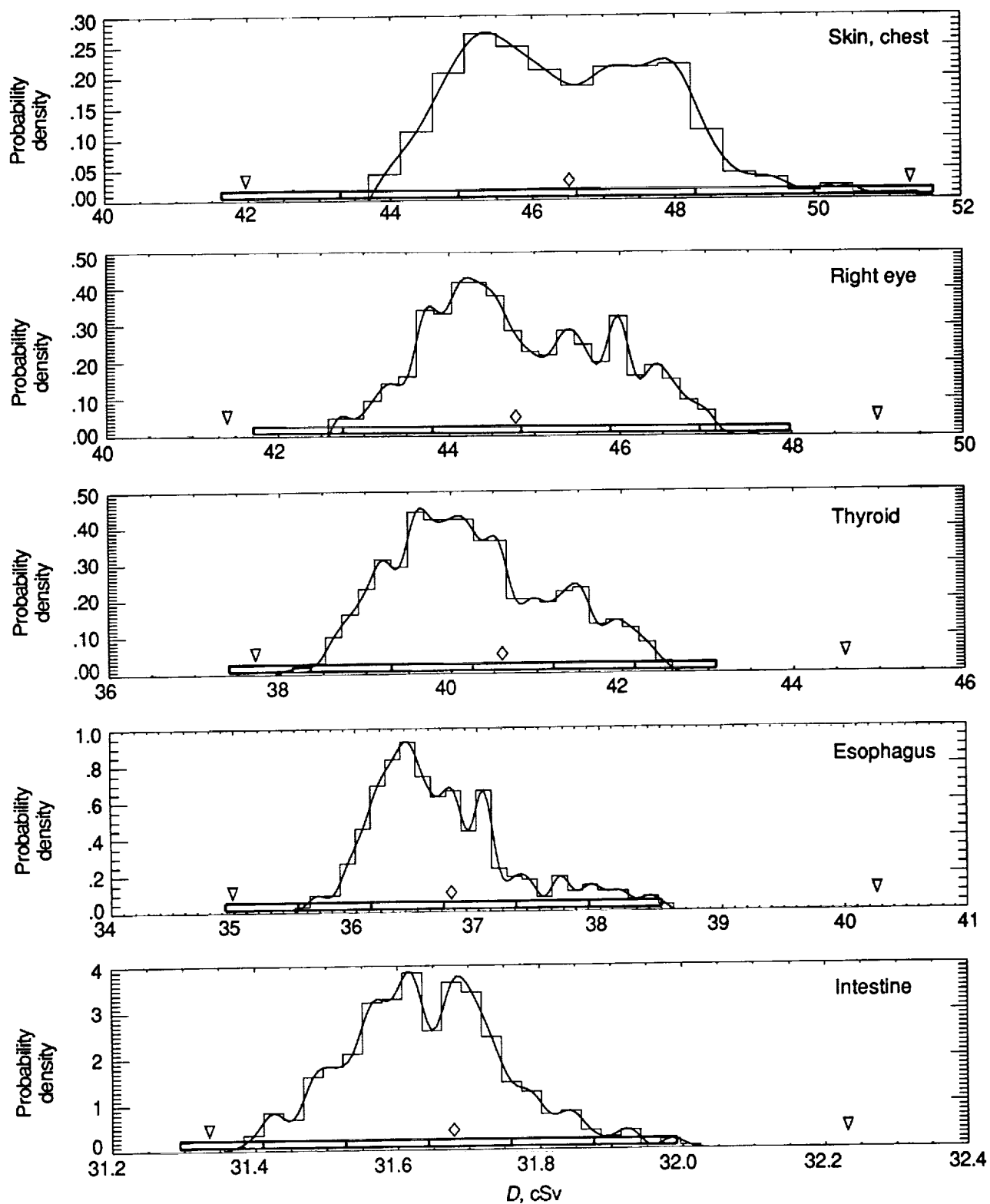
Figure 13. Continued.
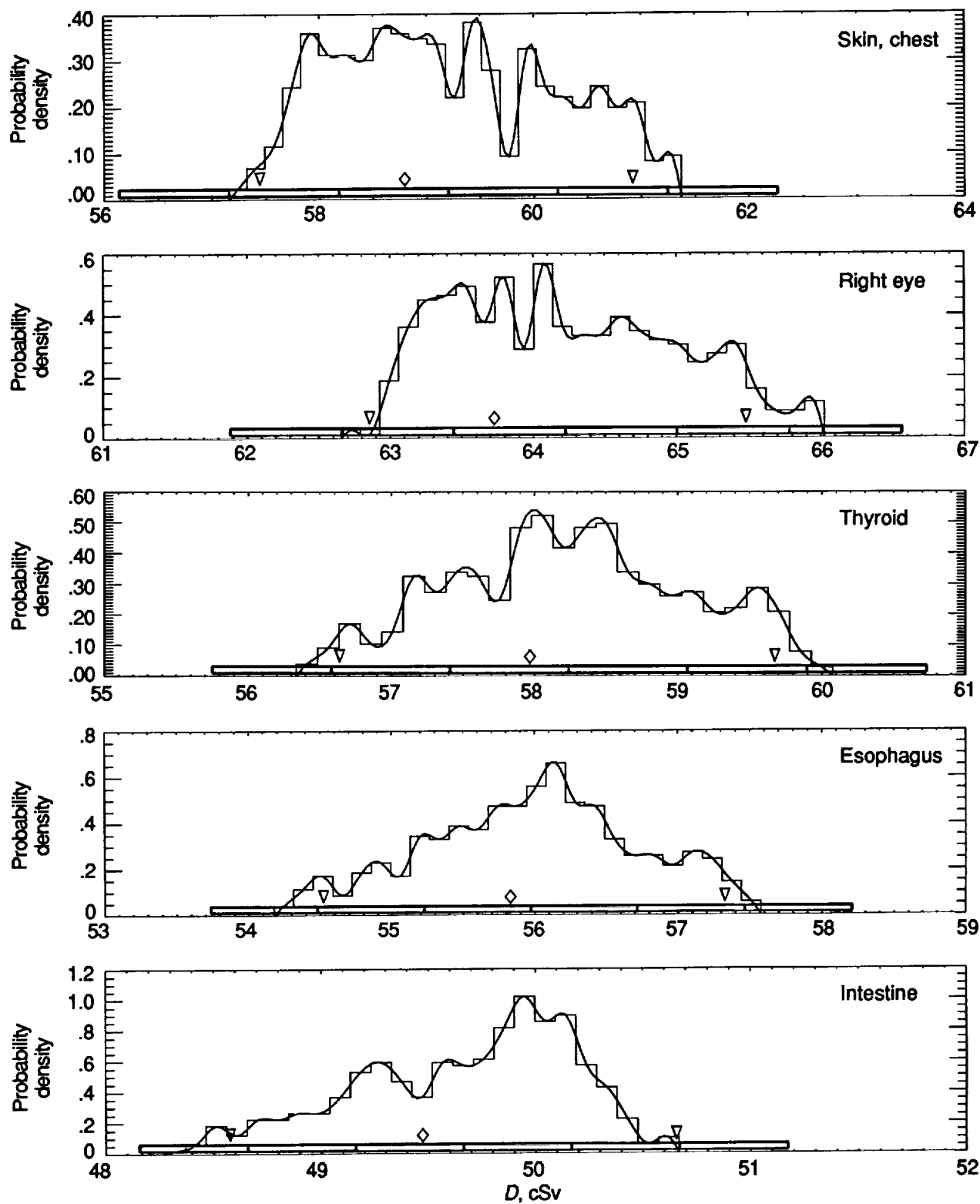
(c) Highly penetrating dose-versus-depth function. $\alpha = 0.04$.
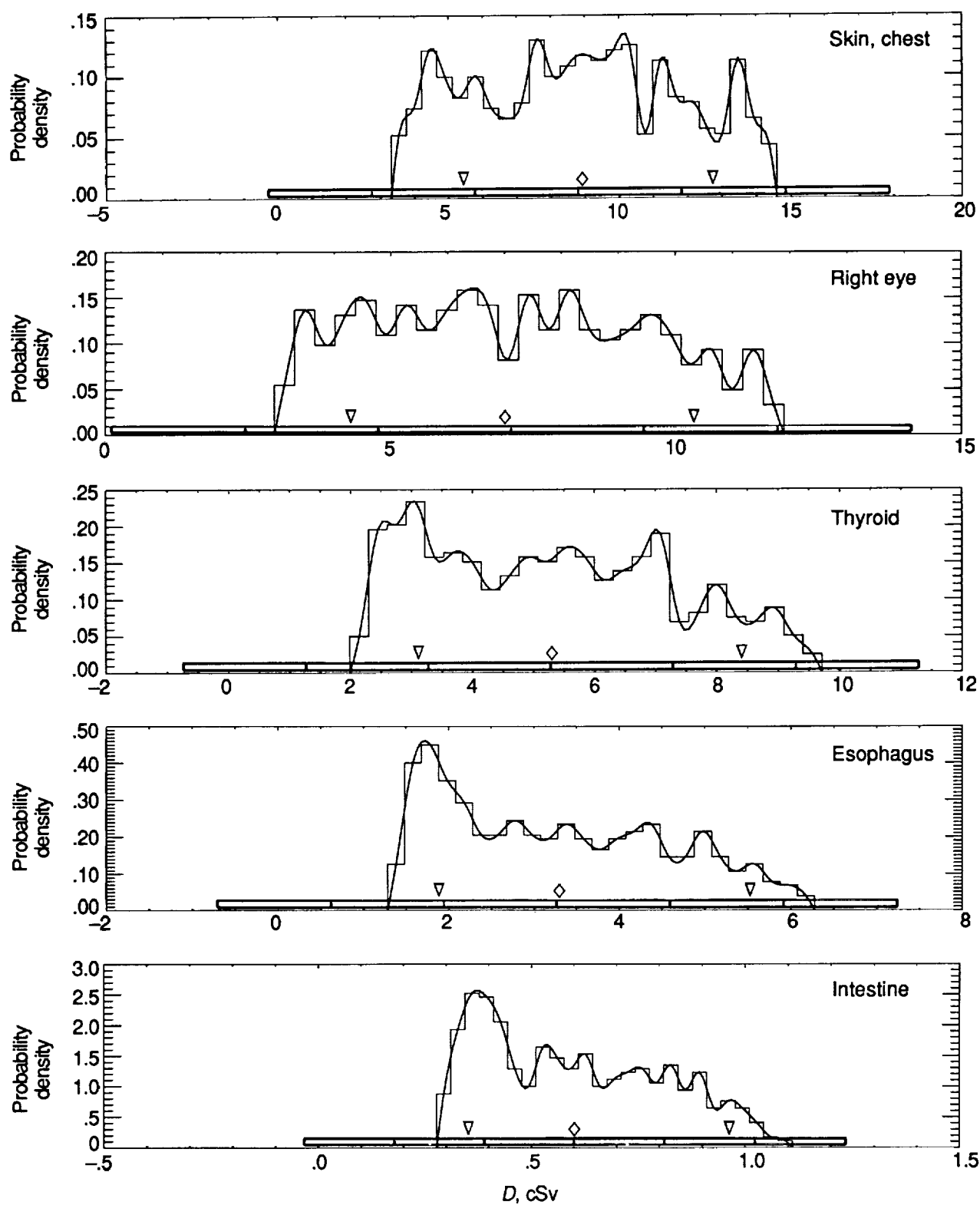
Figure 13. Continued.
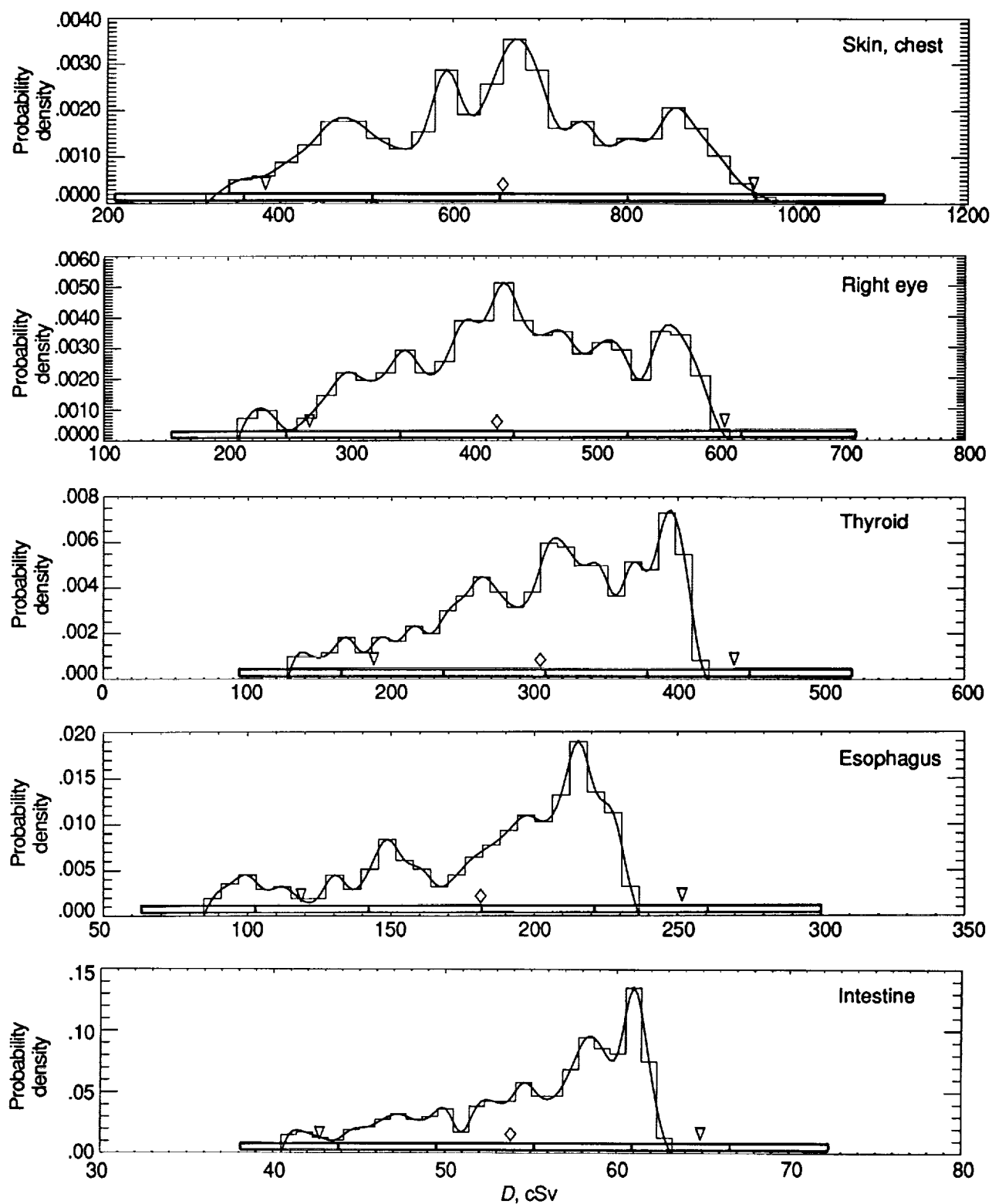
(d) October 1989 proton flare dose-versus-depth function.
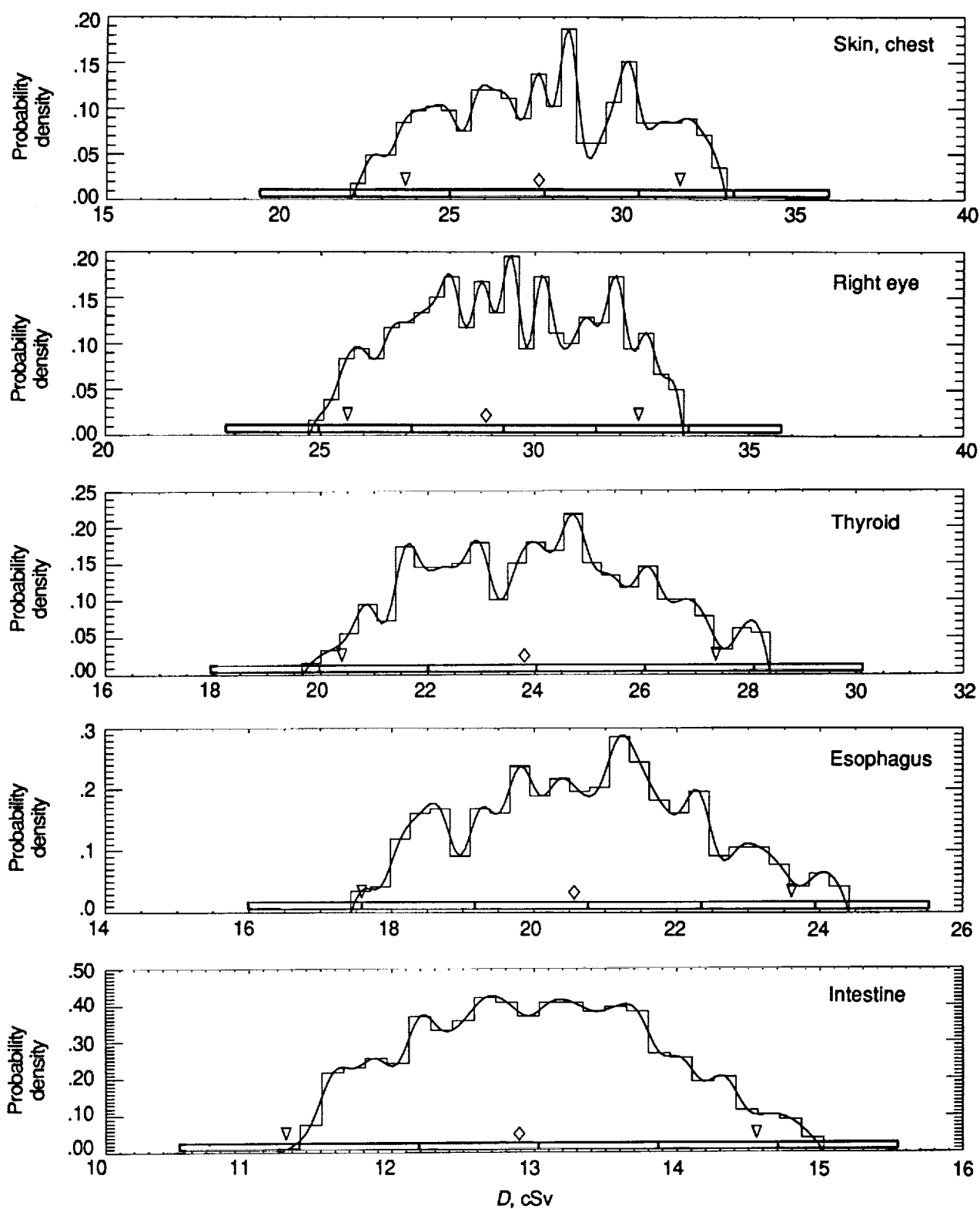
Figure 13. Continued.
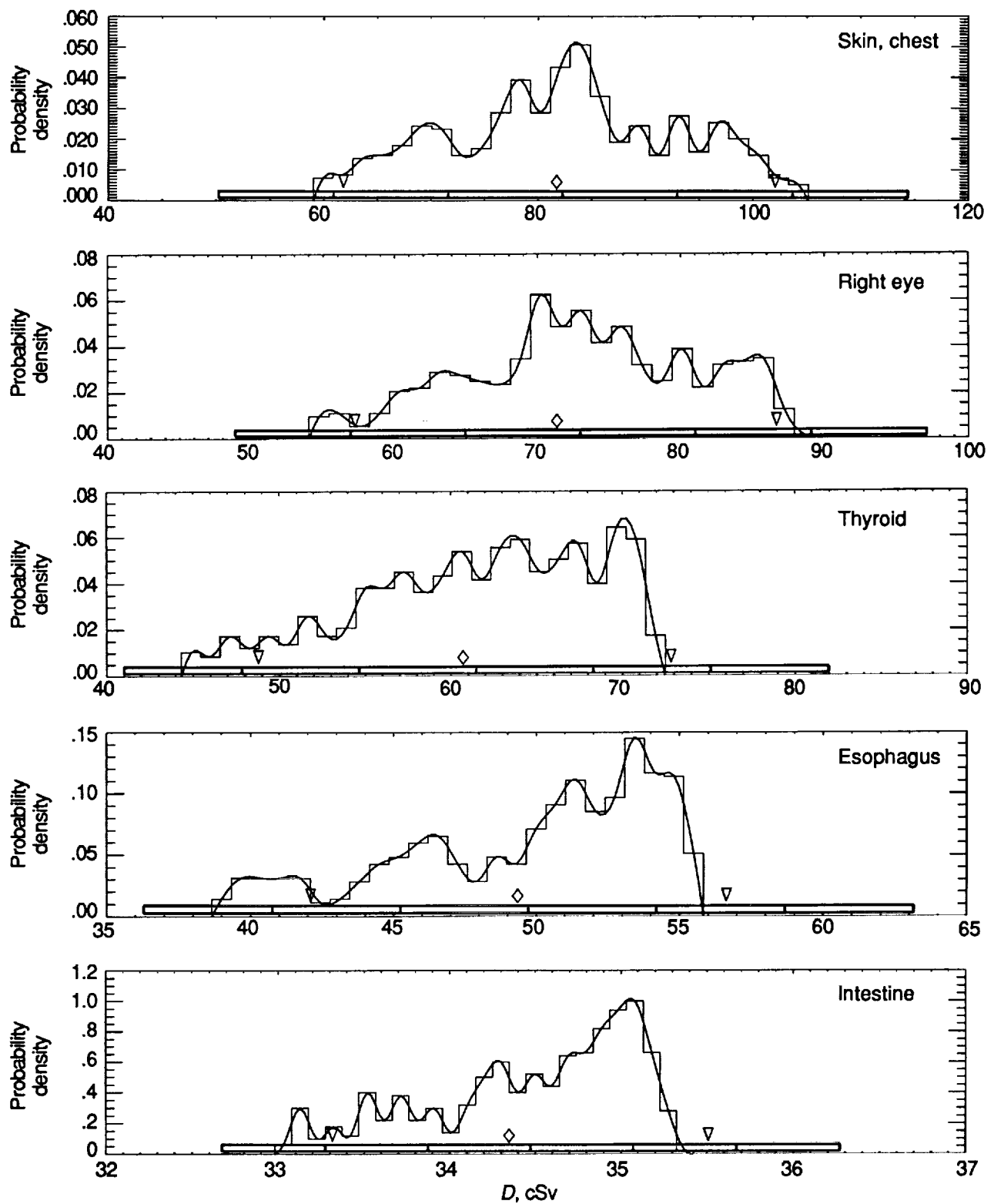
(e) February 1956 proton flare dose-versus-depth function.
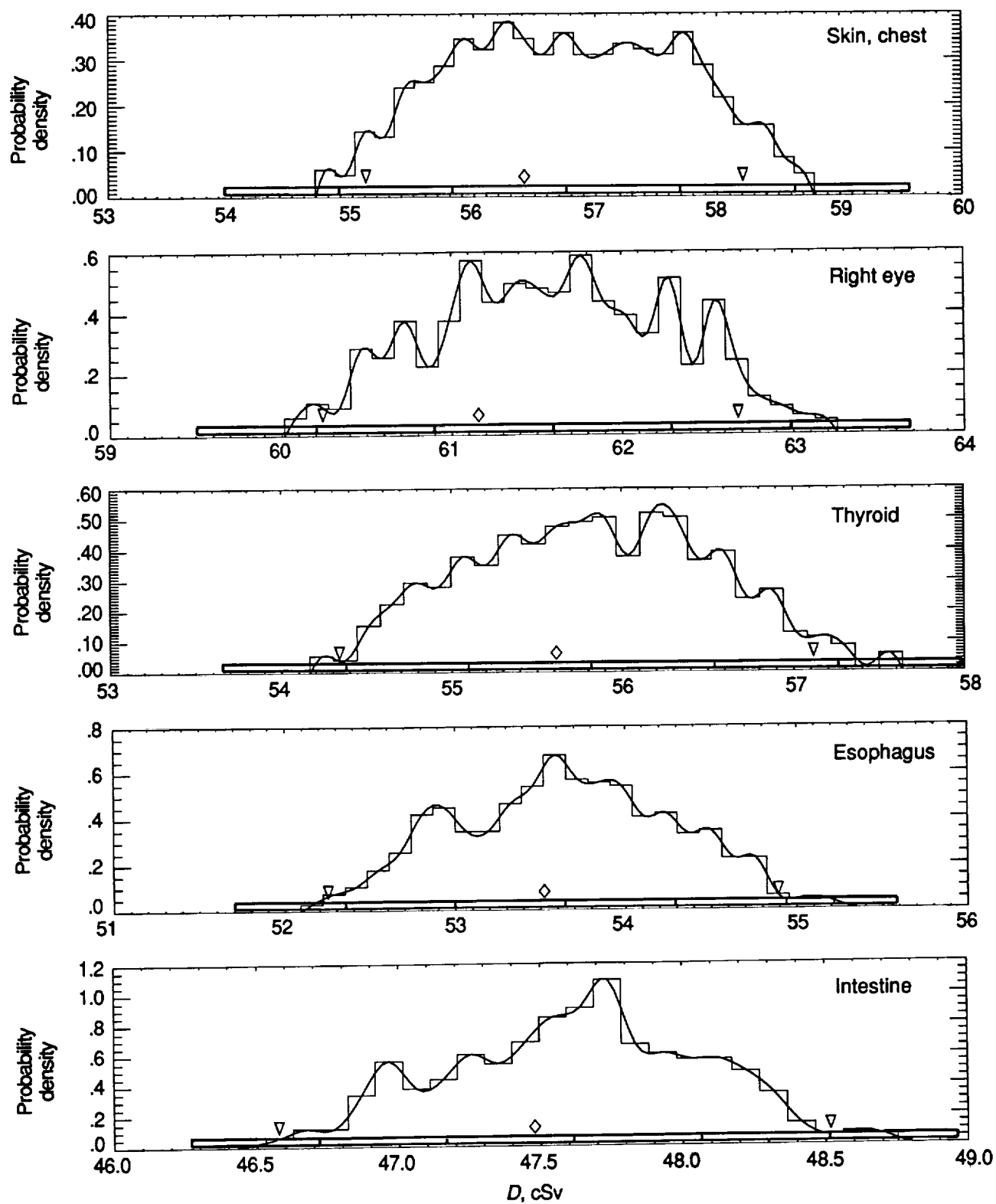
Figure 13. Concluded.
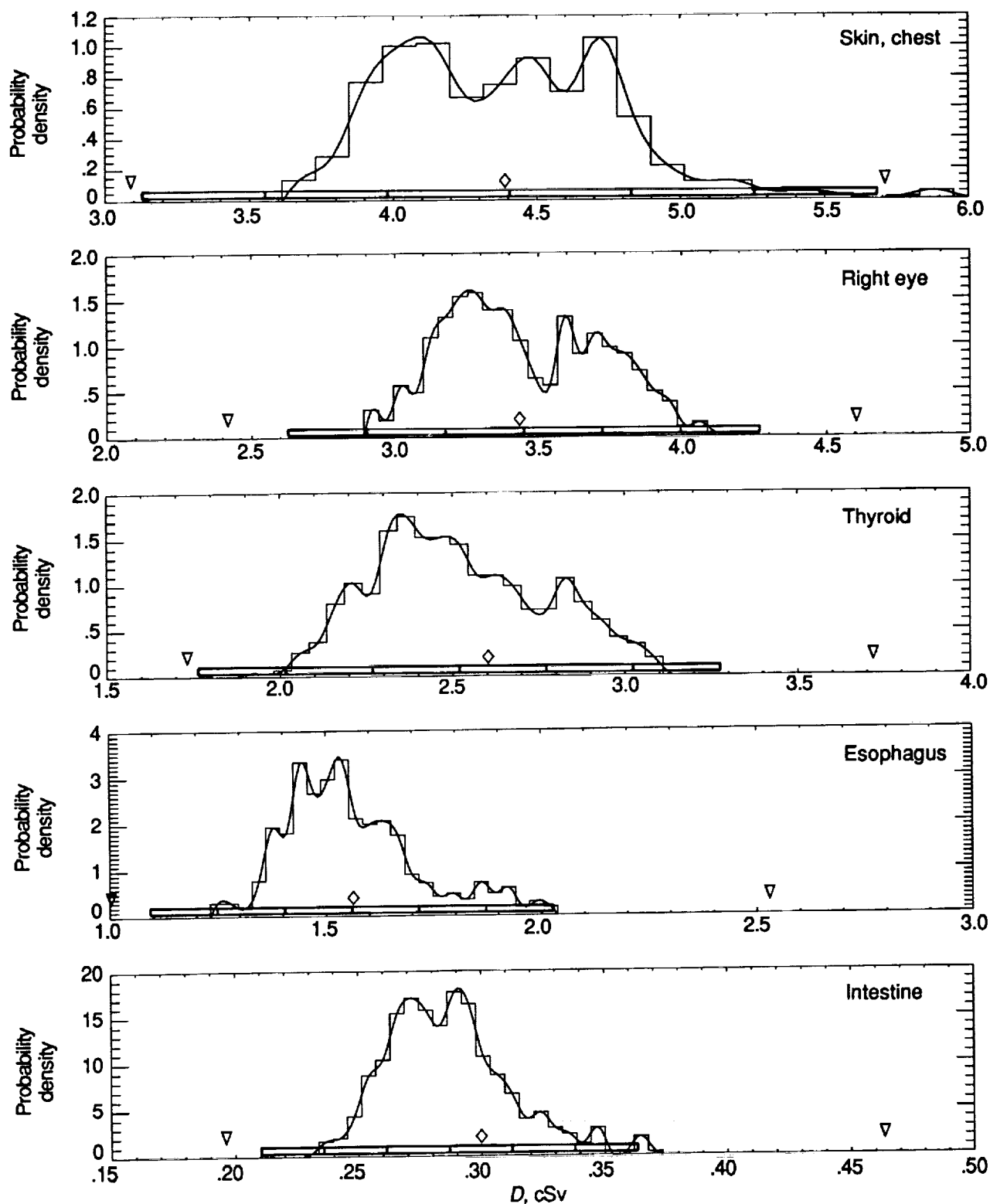
(a) Highly attenuating dose-versus-depth function. $\alpha = 0.4$.

Figure 14. Dose probability density functions for body target points randomly oriented within simulated habitat at point B.
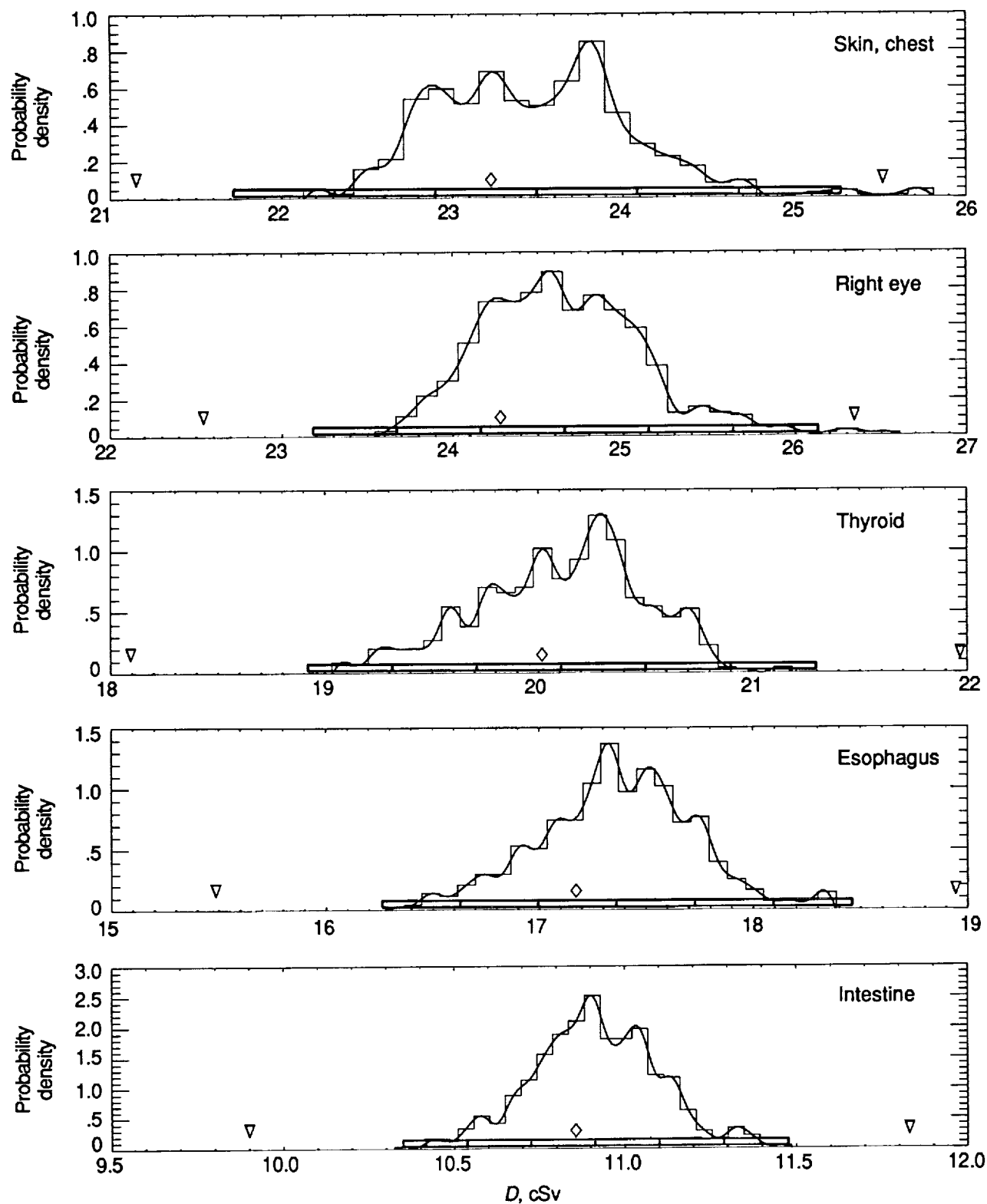
(b) Moderately attenuating dose-versus-depth function. $\alpha = 0.1265$.

Figure 14. Continued.
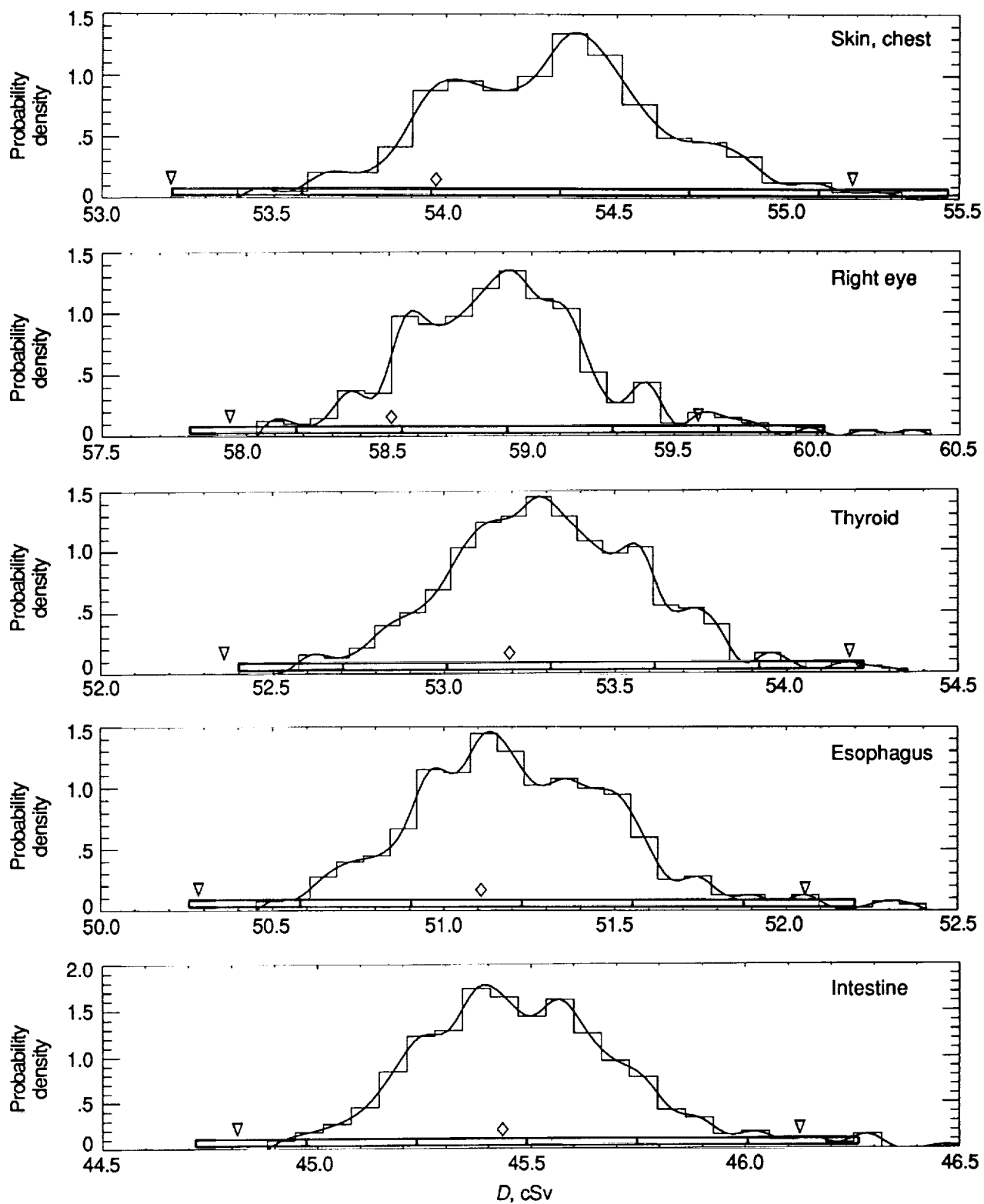
(c) Highly penetrating dose-versus-depth function. $\alpha = 0.04$.

Figure 14. Continued.

(d) October 1989 proton flare dose-versus-depth function.

Figure 14. Continued.

(e) February 1956 proton flare dose-versus-depth function.

Figure 14. Concluded.

(a) Highly attenuating dose-versus-depth function. $\alpha = 0.4$.

Figure 15. Dose probability density functions for body target points randomly oriented within simulated habitat at point C.
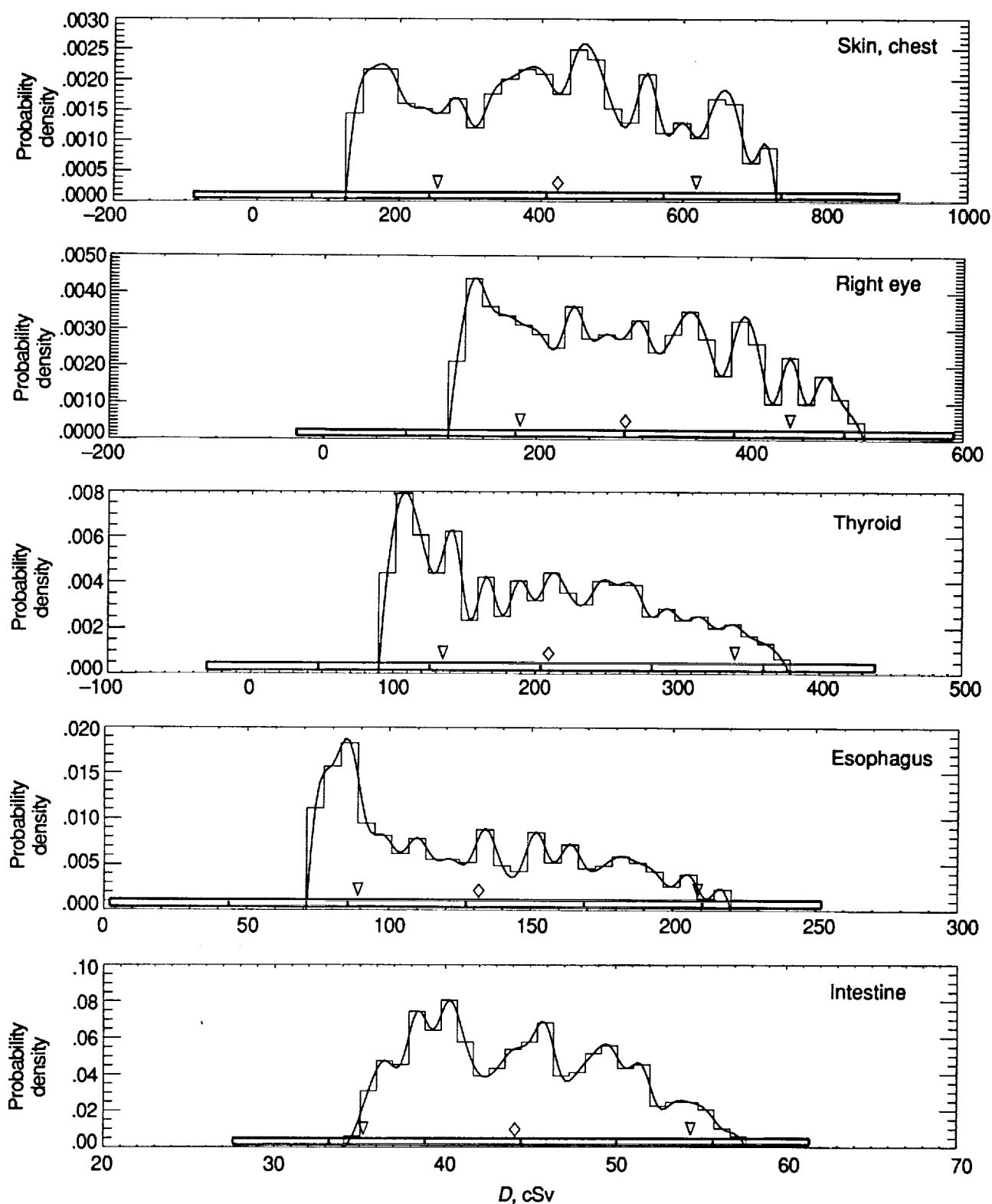
(b) Moderately attenuating dose-versus-depth function. $\alpha = 0.1265$.
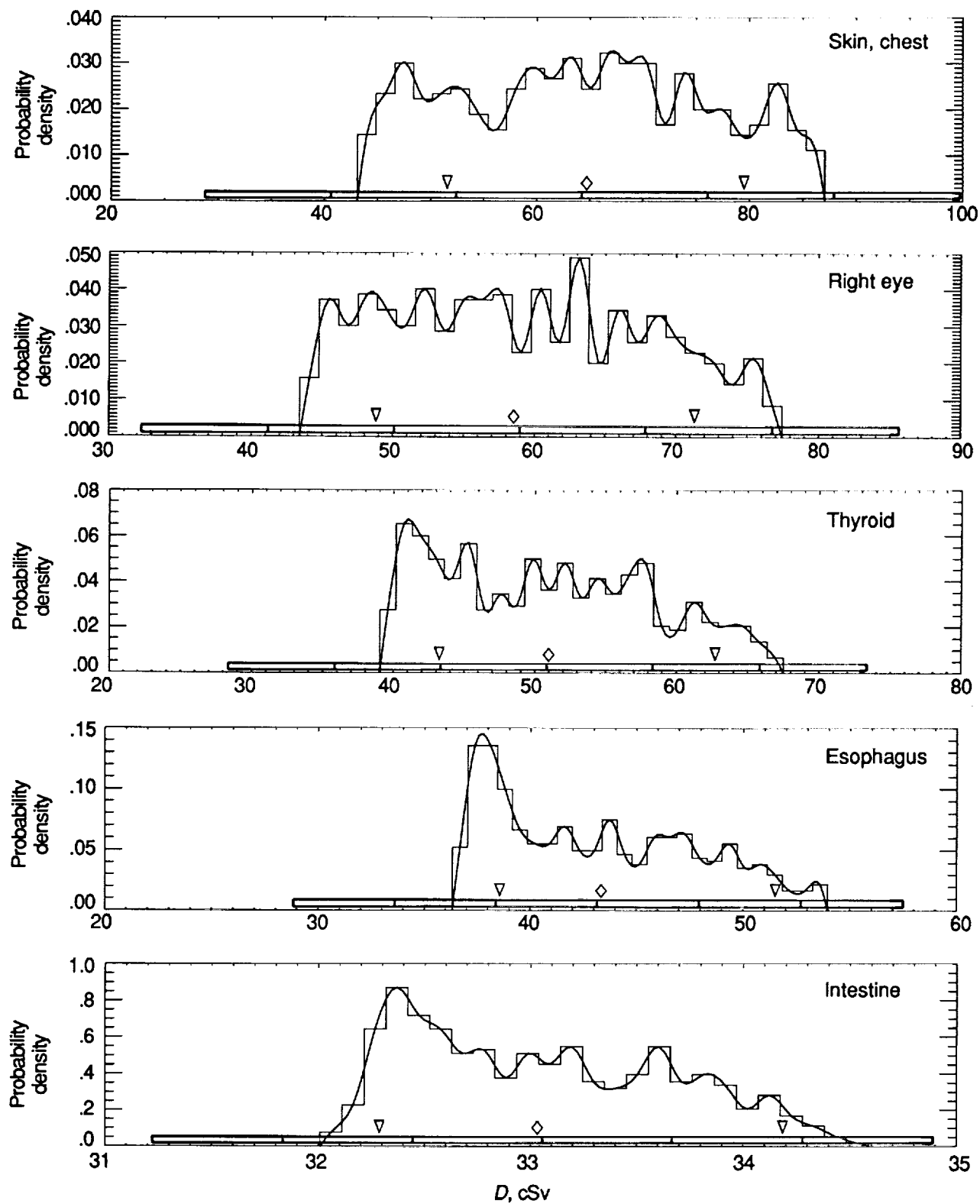
Figure 15. Continued.

(c) Highly penetrating dose-versus-depth function. $\alpha = 0.04$.

Figure 15. Continued.

(d) October 1989 proton flare dose-versus-depth function.

Figure 15. Continued.

(e) February 1956 proton flare dose-versus-depth function.

Figure 15. Concluded.

REPORT DOCUMENTATION PAGE

1. AGENCY USE ONLY *(Leave blank)*	2. REPORT DATE September 1993	3. REPORT TYPE AND DATES COVERED Technical Paper

4. TITLE AND SUBTITLE
Exposure Fluctuations of Astronauts Due to Orientation

5. FUNDING NUMBERS
WU 199-45-16-11

6. AUTHOR(S)
John W. Wilson, John E. Nealy, James S. Wood, Gary Qualls, William Atwell, Judy L. Shinn, and Lisa C. Simonsen

7. PERFORMING ORGANIZATION NAME(S) AND ADDRESS(ES)
NASA Langley Research Center
Hampton, VA 23681-0001

8. PERFORMING ORGANIZATION REPORT NUMBER
L-17254

9. SPONSORING/MONITORING AGENCY NAME(S) AND ADDRESS(ES)
National Aeronautics and Space Administration
Washington, DC 20546-0001

10. SPONSORING/MONITORING AGENCY REPORT NUMBER
NASA TP-3364

11. SUPPLEMENTARY NOTES
Wilson, Nealy, Shinn, and Simonsen: Langley Research Center, Hampton, VA; Wood and Qualls: FMC, Inc., Hampton, VA; Atwell: Rockwell Aerospace, Houston, TX.

12a. DISTRIBUTION/AVAILABILITY STATEMENT

Unclassified–Unlimited

Subject Category 93

12b. DISTRIBUTION CODE

13. ABSTRACT *(Maximum 200 words)*
The dose incurred in an anisotropic environment depends on the orientation of the astronaut's body relative to the direction of the radiation field. The fluctuations in exposure of specific organs due to astronaut orientation are found to be a factor of 2 or more in a typical space habitation module and typical space radiations. An approximation function is found that overestimates astronaut exposure in most cases studied and is recommended as a shield design guide for future space missions.

14. SUBJECT TERMS
Astronauts; Radiation; Shielding

15. NUMBER OF PAGES
52

16. PRICE CODE
A04

17. SECURITY CLASSIFICATION OF REPORT Unclassified	18. SECURITY CLASSIFICATION OF THIS PAGE Unclassified	19. SECURITY CLASSIFICATION OF ABSTRACT	20. LIMITATION OF ABSTRACT